

# AnySurf: Any Surface Generation with Directed Edge

WENDA SHI, The Hong Kong Polytechnic University, Hong Kong SAR

CHENYUAN PAN, PhantomSystem AI, China

DENGMING ZHANG, Zhejiang University, China

YIREN SONG, National University of Singapore, Singapore

BIAO ZHANG, Xi'an Jiaotong University, China

XINGXING ZOU\*, The Hong Kong Polytechnic University, Hong Kong SAR

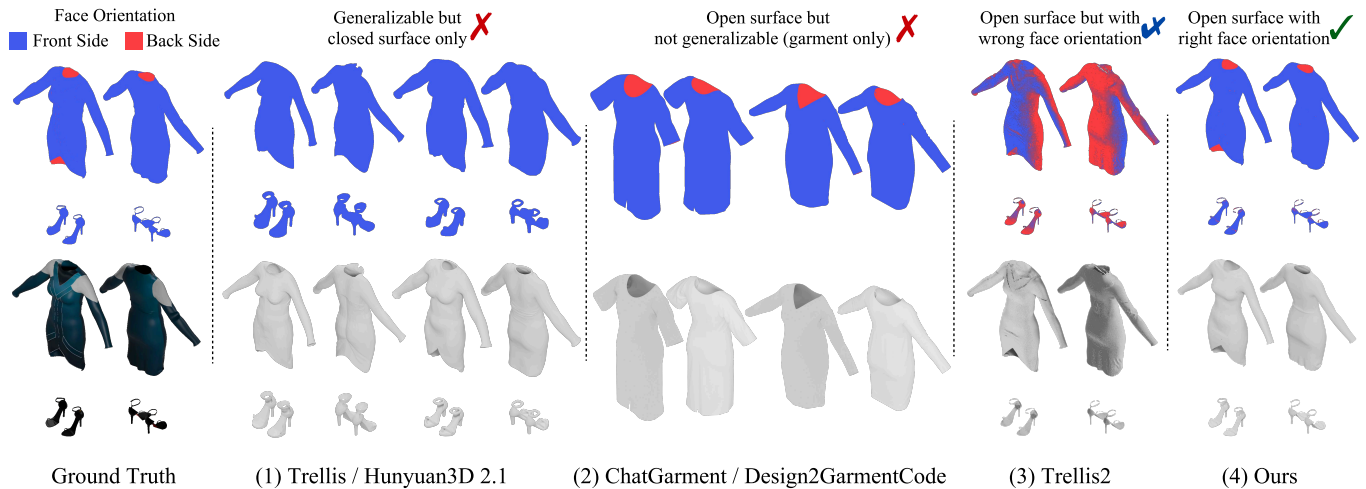


Fig. 1. Comparison of methods for generating 3D outfits that combine open surfaces (e.g., garments) and closed surfaces (e.g., shoes and accessories). (1) General-purpose 3D models (Trellis, Hunyuan3D 2.1) are limited to closed (watertight) surfaces. (2) Garment-specific models (ChatGarment, Design2GarmentCode) handle open surface (non-watertight) garment well but do not extend to closed objects such as shoes and accessories. (3) Trellis2 can produce hybrid open-closed geometry but exhibits inconsistent face orientation. (4) Our method yields hybrid geometry with consistent face orientation, most closely matching the ground truth and suitable for downstream applications.

Open surface components are widely encountered in practical 3D content for real-world industrial pipelines, and they are essential for downstream applications including rendering, physical simulation, and geometric editing. As a representative open surface category, garments have become a natural entry point, and many prior efforts focus on garment generation. These methods have made steady progress with domain-specific representations—e.g., sewing patterns—that split the generation process into 2D pattern prediction

\*Corresponding author

Authors' Contact Information: Wenda Shi, wenda-stone.shi@connect.polyu.hk, The Hong Kong Polytechnic University, Hong Kong SAR; Chenyuan Pan, tpoto1919@gmail.com, PhantomSystem AI, Shanghai, China; Dengming Zhang, dmz@zju.edu.cn, Zhejiang University, Hangzhou, China; Yiren Song, songyiren@sjtu.edu.cn, National University of Singapore, Singapore; Biao Zhang, biao.z@outlook.com, Xi'an Jiaotong University, Xi'an, China; Xingxing Zou, xingxing.zou@polyu.edu.hk, The Hong Kong Polytechnic University, Hong Kong SAR.

Permission to make digital or hard copies of all or part of this work for personal or classroom use is granted without fee provided that copies are not made or distributed for profit or commercial advantage and that copies bear this notice and the full citation on the first page. Copyrights for components of this work owned by others than the author(s) must be honored. Abstracting with credit is permitted. To copy otherwise, or republish, to post on servers or to redistribute to lists, requires prior specific permission and/or a fee. Request permissions from [permissions@acm.org](mailto:permissions@acm.org).

© 2018 Copyright held by the owner/author(s). Publication rights licensed to ACM.

ACM 1557-7368/2018/8-ART111

<https://doi.org/XXXXXXX.XXXXXXX>

followed by physics-based 3D stitching. However, such specialized representation limits scalability and generalization beyond garments, making it difficult to handle broader asset categories such as shoes and accessories. Moreover, most general-purpose 3D generators rely on field-based representations and iso-surfacing, which favor watertight meshes and often fail on open surfaces, producing thin double-layer shells. Trellis2 is a key step forward with a field-free, general 3D representation, yet its open surface outputs still suffer from normal and topology defects.

To address these limitations, we propose *AnySurf*, a unified pipeline for open, closed and hybrid surface 3D assets generation while maintaining faithful face orientation. At its core is *FDG-D*, a directed-edge extension of the Flexible Dual Grid (FDG) representation that preserves critical normal-orientation cues by assigning a direction to each surface-intersecting grid edge. We further introduce a post-training strategy *ROS-FT*, together with a lightweight, plug-and-play *DE-Adapter* that adds only about 1% more parameters, enabling the model to learn directed edges without compromising its original generative capabilities. Finally, we present *Outfit3D*, a hybrid dataset comprising industry-level open-surface garments and closed-surface accessories. Our approach thus redefines 3D garment modeling, evolving it from a *domain-specific* task into an integral part of the *general* 3D generative landscape. Experiments show that our method outperforms baselines, yielding meshes that are more practical for downstream tasks. We will make our datasets, code, and models publicly available.

CCS Concepts: • **Do Not Use This Code** → **Generate the Correct Terms for Your Paper**; *Generate the Correct Terms for Your Paper*; Generate the Correct Terms for Your Paper; Generate the Correct Terms for Your Paper.

Additional Key Words and Phrases: Do, Not, Use, This, Code, Put, the, Correct, Terms, for, Your, Paper

#### ACM Reference Format:

Wenda Shi, Chenyuan Pan, Dengming Zhang, Yiren Song, Biao Zhang, and Xingxing Zou. 2018. AnySurf: Any Surface Generation with Directed Edge. *ACM Trans. Graph.* 37, 4, Article 111 (August 2018), 17 pages. <https://doi.org/XXXXXXX.XXXXXXX>

## 1 Introduction

Production-grade 3D assets are often *hybrid*, combining closed volumetric surfaces and open surfaces without volumetric enclosure. Accordingly, a practical 3D generation model ought to produce downstream-ready meshes tailored for rendering, physical simulation, geometric editing, and digital manufacturing. However, faithfully modeling open surface components, namely non-watertight geometries, remains a long-standing technical challenge, despite their widespread presence in high-value scenarios. Typical use cases include garments and soft goods (e.g., cloth simulation, virtual try-on, and physical fabrication), foliage and plant structures for large-scale environment reconstruction, as well as thin-walled industrial and precision components such as gaskets, seals, stamped metal parts, and thin protective housings. In particular, garments stand out as the most representative category of open-surface 3D assets.

For thin garment modeling, sewing-pattern based methods are among the most popular: they leverage LLMs/VLMs to synthesize planar patterns (often in SVG-like formats) and stitch them into 3D garments, naturally guaranteeing open surfaces. Some use autoregressive or diffusion frameworks to either generate vectorized [He et al. 2024; Li et al. 2025d; Liu et al. 2025; Nakayama et al. 2024] or rasterized [Tatsukawa et al. 2025] sewing patterns together with edge-wise sewing correspondences and 3D initializations as per-pattern rigid-transformation matrices, or emit high-level parameters [Bian et al. 2025; Guo et al. 2025] and programs [Zhou et al. 2025] of a parametric pattern-making DSL such as GarmentCode [Korostelova and Sorkine-Hornung 2023]. The generated patterns are then draped onto a target avatar using conventional cloth simulation. While this paradigm preserves structural correctness by explicitly producing sewing patterns, it lacks full spatial context and often fails to reproduce fine folds and realistic drape geometry. GarmageNet [Li et al. 2025c] propose a novel garment representation that encodes each pattern as a structured geometry image, effectively bridging the semantic and geometric gap between 2D structural patterns and 3D garment geometries, and with a latent diffusion transformer to synthesize pattern-wise geometry images. However, these *domain-specific* representations struggle to generalize beyond garments. The broader challenge of synthesizing arbitrary 3D assets—particularly combination of open and closed surfaces like full outfits with accessories—remains an open problem.

In parallel, general-purpose 3D generation methods [Achlioptas et al. 2018; Chan et al. 2021; Gu et al. 2022; Li et al. 2023b; Liu et al. 2024b, 2023a; Long et al. 2023a; Luo and Hu 2021] aim

Methods	Closed Surface [General Object]	Open Surface [Thin Garment]	Hybrid Surface [eg. Outfits]
Design2garment [CVPR 25]	✗	✓	✗
ChatGarment [CVPR 25]	✗	✓	✗
DressItto3 [SIGGRAPH 25]	✗	✓	✗
DMap [SIGGRAPH 25]	✗	✓	✗
SewingLDM [ICCV 25]	✗	✓	✗
GarmageNet [SIG'Aisa 25]	✗	✓	✗
Trellis [CVPR 25]	✓	✗	✗
Hi3DGen [ICCV 25]	✓	✗	✗
Step1X-3D [ArXiv 25]	✓	✗	✗
Hunyuan-3D 2.1 [ArXiv 25]	✓	✗	✗
Trellis2 [CVPR 26]	✓	✓	✓
Ours	✓+ FO	✓+ FO	✓+ FO

Table 1. Differences with existing 3D generation methods, classified into thin garment and general object generation. FO means face orientation.

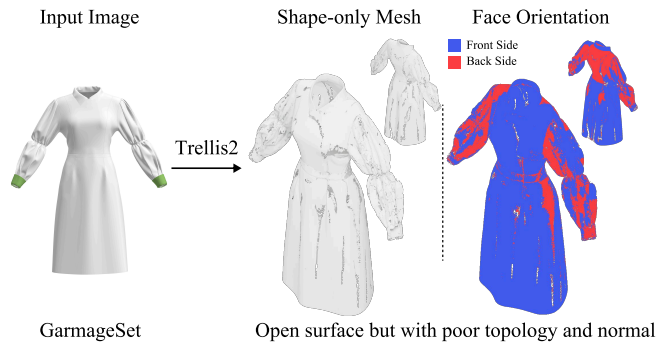


Fig. 2. Textureless results of Trellis2 on open surface data (eg, GarmageSet).

to synthesize diverse shapes beyond garments and other domain-specific categories. They build on a range of representations, including point clouds [Achlioptas et al. 2018; Luo and Hu 2021], voxel grids [Smith and Meger 2017; Xie et al. 2018], and implicit fields such as SDFs [Chen and Zhang 2019; Mittal et al. 2022]. While point- and voxel-based representations make surface extraction challenging, implicit fields are particularly effective for watertight shapes; supporting open surfaces and complex topologies remains difficult even with improved formulations (e.g., 3PSDF [Chen et al. 2022a] and TSDF [Sun et al. 2021]) or alternative open surface representations (e.g., G-Shell and Surf-D [Liu et al. 2024a; Yu et al. 2025]). Meanwhile, recent large-scale systems [Tochilkin et al. 2024; Xiang et al. 2025b; Zhang et al. 2024b; Zhao et al. 2025] explore more scalable latent representations (e.g., VecSet [Zhang et al. 2023b] or structured latents [Xiang et al. 2025b]) with diffusion transformers, substantially improving generalization—yet the generation of open surface geometry remains a bottleneck.

This limitation is not merely a modeling gap but also a representation bottleneck. Most general-purpose 3D generative models [Hunyuan3D et al. 2025; Jia et al. 2025; Li et al. 2025g; Xiang et al. 2025b] ultimately rely on *field-based* shape representations (e.g., SDFs) followed by iso-surfacing (e.g., Marching Cubes/Flexible Cubes [Lorensen and Cline 1998; Shen et al. 2023]), a pipeline intrinsically biased toward watertight closed surfaces. Geometry without volume is therefore hard to represent faithfully, and open surface structures often collapse into extremely thin yet still closed *double-layer shells*. For garments, such “thick” watertight shells introduce multiple nearly coincident layers, making near-contact collision handling ill-conditioned and prone to interpenetration.

To solve this problem, Trellis2 [Xiang et al. 2025a] marks a key turning point by introducing a *field-free* and *general* representation, breaking the long-standing dependence on fields and iso-surfacing while retaining generality. However, as shown in Fig. 2, its generated open surface garment suffer from inconsistent face orientation and topological defects (e.g., non-manifoldness and local connectivity issues). This reveals a critical issue: even when a mesh is nominally open, inconsistent normals can be catastrophic. They not only break the appearance (shading and material response) but also severely destabilize downstream physics-based simulation and geometry processing. Therefore, our goal is to enable *general* 3D generation that supports open surfaces with reliable face orientation, without sacrificing the inherent generative capabilities of base models.

To achieve this goal, we propose a new 3D representation *FDG-D* (Flexible Dual Grid with Directed Edge) that preserves normal information during dualization. We also propose a post-training strategy, *ROS-FT* (Real Open Surface Fine-Tuning), with a plug-and-play *DE-Adapter* (Directed Edge Adapter) to learn directed edges while keeping the base model’s capabilities. Finally, we introduce a hybrid dataset, *Outfit3D*, to evaluate mixed open/closed assets rather than only pure open surfaces. Our contributions are summarized:

- *AnySurf* framework. A unified 3D generation pipeline capable of synthesizing any 3D surface (open, closed, or hybrid) with correct face orientation. This establishes a new paradigm for garment modeling, shifting the field from domain-specific workflows toward universal 3D generative pipelines.
- *FDG-D* representation. A minimal yet effective 3D representation that explicitly encodes directed edges, enabling robust reconstruction and generation of arbitrary surfaces while preserving consistent face orientations.
- *ROS-FT* strategy & *DE-Adapter*. A progressive post-training strategy equipped with a lightweight module (adding only 1.16% parameters) to restore face orientation without compromising the powerful generative priors of the base model.
- *Outfit3D* dataset. The first comprehensive hybrid dataset containing both open surfaces (thin garments) and closed surfaces (accessories), featuring industry-level high-precision outfits with textures and UV (2D patterns) information.
- Extensive Evaluation. We conduct experiments and ablation studies against existing baselines, demonstrating the superiority and effectiveness of our proposed method across diverse topological domains.

## 2 Related Works

### 2.1 Garment Generation

Garments are a representative and practically important domain for open surface generation. Existing approaches can be organized into three paradigms: *pattern-based* methods that explicitly model 2D sewing patterns and seams, *geometry-based* methods that directly synthesize 3D garment surfaces, and hybrid *pattern+geometry* methods that jointly generate both patterns and surface initialization.

*Pattern-based* pipelines typically proceed in two stages: they first predict 2D patterns and seam connectivity as sewing patterns, and then stitch patterns along seams and drape them on a target avatar with cloth simulation. Depending on the 2D pattern representation,

prior work falls into three families. (i) Vector-quantization (VQ) methods cast pattern prediction as sequence modeling over discrete 1D tokens. NeuralTailor [Korosteleva and Lee 2022] reconstructs patterns from unstructured point clouds with an LSTM decoder and point-level attention; later work expands inputs (text in DressCode [He et al. 2024], images in SewFormer [Liu et al. 2023b]) and couples prediction with differentiable simulation so that simulated drape matches the image [Li et al. 2025e]. Diffusion-based [Li et al. 2025d; Liu et al. 2023b] and LLM-based [Nakayama et al. 2024] variants further scale the VQ formulation to larger, more complex GarmentCodeData and more modalities. (ii) Template-based methods address structural validity (e.g., seam correctness) by targeting GarmentCode [Korosteleva and Sorkine-Hornung 2023] and generating high-level parameters or DSL programs [Bian et al. 2025; Guo et al. 2025; Zhou et al. 2025] to enforce constraints and improve pattern quality. (iii) Image-based encodings preserve the 2D layout of patterns via explicit [Chen et al. 2022c; Tatsukawa et al. 2025] or implicit [Li et al. 2024d] raster representations. The extra capacity supports UV-aligned maps of 3D drape [Li et al. 2025a, 2024b,c] and pairs naturally with modern image generative models [Gu et al. 2002; Yan et al. 2024; Yu and Wang 2024], at the cost of redundancy.

*Geometry-based* methods skip explicit patterns and model garment geometry directly in 3D. Implicit approaches use unsigned distance fields (UDF) [Chen et al. 2024c; Yu et al. 2025], manifold distance fields [Liu et al. 2024a], or Gaussian splatting [Liu et al. 2024c; Rong et al. 2025], often with diffusion or GAN-based generators for plausible assets and dynamics [Rong et al. 2025; Xie et al. 2024]. Extracting usable triangle or quad meshes from these representations still leans on iso-surface extraction, which is fragile for thin sheets with open boundaries. Another family deforms a fixed garment template and registers it to an avatar via optimization [Qiu et al. 2023; Zhu et al. 2022] or differentiable simulation [Li et al. 2024a; Sarafianos et al. 2024]; although the topology stays controlled, but expressiveness is limited by the template itself.

*Dual-stream (Pattern+geometry)* methods aim to jointly generate patterns, sewing seam, and a 3D initialization compatible with physics-based simulation. For example, [Li et al. 2025c] proposes a unified framework that automates 2D pattern creation, seam construction, and 3D garment initialization, following [Yan et al. 2025].

Overall, although these methods are able to generate open surfaces (thin garments), but garment-specific pipelines rely on domain-tailored structure (pattern–seam programs, pattern tokenizations, or fixed garment templates), which restricts scalable training data and can hurt generalization relative to more general 3D generators.

### 2.2 General Object Generation

General-purpose 3D generation has witnessed a paradigm shift, evolving through distinct representational and architectural stages to synthesize diverse, high-fidelity assets beyond domain-specific categories. This evolution can be categorized into three stages.

*Stage 1: Early Generative Models.* Initially, 3D generation methods [Achlioptas et al. 2018; Chan et al. 2021; Gu et al. 2022; Li et al. 2023b; Liu et al. 2024b, 2023a; Long et al. 2023a; Luo and Hu 2021] predominantly relied on explicit, discrete representations, such as point clouds [Achlioptas et al. 2018; Luo and Hu 2021] and voxel

grids [Smith and Meger 2017; Xie et al. 2018]. While intuitive, these structures often struggle with high-resolution surface extraction. To address this, implicit fields—particularly Signed Distance Functions (SDFs) [Chen and Zhang 2019; Mittal et al. 2022]—emerged as the standard paradigm. Implicit fields are exceptionally effective for ensuring continuous, watertight geometries, demonstrating unprecedented quality in closed surface modeling.

*Stage 2: Shift to Diffusion Transformers.* As 2D image synthesis pivoted toward scalable architectures, 3D generation similarly adopted Diffusion Transformers (DiTs) as a milestone breakthrough. Moving beyond localized U-Net structures, pioneering works such as DiT-3D explored plain transformers for high-fidelity shape generation by directly denoising voxelized point clouds, demonstrating superior scalability and structural coherence. This transition enabled the integration of structured latent spaces (e.g., VecSet [Zhang et al. 2023b] or sparse voxels [Xiang et al. 2025b]) capable of decoding into multiple output formats, including radiance fields, 3D Gaussians, and explicit meshes [Liu et al. 2024b; Tochilkin et al. 2024], serving as a fundamental paradigm shift in 3D generation.

*Stage 3: Large-Scale 3D Foundation Models.* This architectural evolution has unfolded alongside the rapid expansion of massive 3D asset datasets (e.g., Objaverse [Deitke et al. 2024, 2023b] and TexVerse [Zhang et al. 2025]). Benefiting from the transformer architecture’s scalability, recent large-scale systems—such as Trellis [Xiang et al. 2025b], Hunyuan3D [Hunyuan3D et al. 2025; Zhao et al. 2025], CLAY [Zhang et al. 2024b], and others [Chen et al. 2024b; Li et al. 2025f,g; Yang et al. 2025a]—leverage billion-parameter backbones to achieve general 3D asset creation with high-quality shapes and textures, improving generalization across diverse categories.

Despite these remarkable advancements, the downstream usability of the generated geometry remains a fundamental bottleneck. Specifically, the prevailing reliance on SDFs or volumetric latents inherently assumes watertight, manifold surfaces. Consequently, even with improved formulations (e.g., 3PSDF [Chen et al. 2022a] and TSDF [Sun et al. 2021]), these state-of-the-art methods systematically struggle to accurately reconstruct and generate thin-shell structures, open surfaces, and complex self-intersecting topologies. While alternative open surface representations—such as G-Shell [Liu et al. 2024a] and Surf-D [Yu et al. 2025]—have been proposed to successfully handle arbitrary topologies including thin garments, their complex formulations (e.g., manifold distance fields or Unsigned Distance Fields) severely limit their scalability. They are computationally intensive and difficult to seamlessly integrate into the massive transformer backbones that drive modern 3D foundation models. This underscores the necessity for new representational paradigms tailored for open surface 3D generation that are both topologically expressive and highly scalable.

### 2.3 3D Representations For Open Surface

Neural implicit functions are a widely used family of 3D representations due to their ability to model surfaces with arbitrary topology. They map query coordinates to occupancy values [Mescheder et al. 2019] or to signed/unsigned distance fields [Chibane et al. 2020; Park et al. 2019], and can be learned from diverse 2D/3D supervision signals [Chen et al. 2024a; Li et al. 2022; Ma et al. 2021; Noda

et al. 2024; Wang et al. 2021]. To better handle open surfaces, which lack a well-defined inside–outside notion, many methods adopt Unsigned Distance Functions (UDFs) and predict the unsigned distance from arbitrary points to the surface [Chibane et al. 2020; Guillard et al. 2022; Long et al. 2023b; Zhang et al. 2024a; Zhou et al. 2024]; recent work further couples UDF learning with 3D Gaussian Splatting for image-based reconstruction, e.g., GaussianUDF [Li et al. 2025b]. However, these pipelines typically require a separate surface extraction stage—often adapting marching cubes [Hou et al. 2023; Kobbelt et al. 2001; Lorenzen and Cline 1998] or dual contouring [Chen et al. 2022b; Ju et al. 2002]—and can be sensitive to sampling and optimization choices, leading to artifacts such as holes, noise, or unstable orientation. Moreover, most prior open surface reconstruction methods are primarily developed for single-object reconstruction training on relatively small 3D object datasets, making it challenging to scale up to general 3D asset generation.

In contrast, recent large-scale models like Trellis2 [Xiang et al. 2025a] leverage native, compact structured latents—specifically, O-Voxel representations featuring a Flexible Dual Grid (FDG) for shape and Volumetric Surface Attributes (VSA) for textures. This allows them to directly represent open surfaces, non-manifold geometry, and internal structures without relying on costly iso-surface extraction, marking a significant step toward versatile, open surface 3D generation. However, the standard FDG formulation inherently discards explicit normal information during the grid construction process. Consequently, the generative model struggles with chaotic and inconsistent face orientations, severely limiting the usability of the generated assets in normal-sensitive downstream applications, such as physics-based simulation and high-quality rendering.

## 3 Motivation

### 3.1 Preliminaries

Prior 3D generative models [Li et al. 2025g; Xiang et al. 2025b; Yang et al. 2024; Zhao et al. 2025] can synthesize complex, high-fidelity meshes, yet most rely on signed distance fields (SDFs) and marching cubes that inherently favor closed, watertight surfaces and thus struggle with open surface geometry. To achieve open surfaces, Trellis2 [Xiang et al. 2025a] introduces a field-free 3D representation *O-Voxel*, consisting of a shape component, *Flexible Dual Grid* (FDG), and a material component, *Volumetric Surface Attributes* (VSA). FDG constructs a dual grid over a regular voxel lattice: it assigns one dual vertex to each active voxel and activates a quadrilateral dual face (quad for short) for each voxel edge intersected by the input mesh, thereby connecting adjacent dual vertices. Inspired by Dual Contouring [Chen et al. 2022b; Ju et al. 2002] but without any underlying scalar field (e.g., an SDF), FDG directly computes mesh–edge intersections and uses the resulting points and normals as Hermite data  $\{q_i, \mathbf{n}_i\}$ . For each active voxel, the dual vertex  $\mathbf{v}$  is obtained by minimizing the quadratic error function (QEF):

$$\min_{\mathbf{v} \in \text{voxel}} e(\mathbf{v}) = \sum_i d_{\Pi,i}^2 + \lambda_{\text{bound}} \sum_j d_{L,j}^2 + \lambda_{\text{reg}} d_{\tilde{q}}^2. \quad (1)$$

Compared with the original Dual Contouring QEF term  $d_{\Pi,i}^2 = (\mathbf{n}_i \cdot (\mathbf{v} - \mathbf{q}_i))^2$ , FDG adds a boundary-alignment term  $d_{L,j}^2$  and a regularizer  $d_{\tilde{q}}^2 = \|\mathbf{v} - \tilde{\mathbf{q}}\|^2$ , improving open surface fidelity while

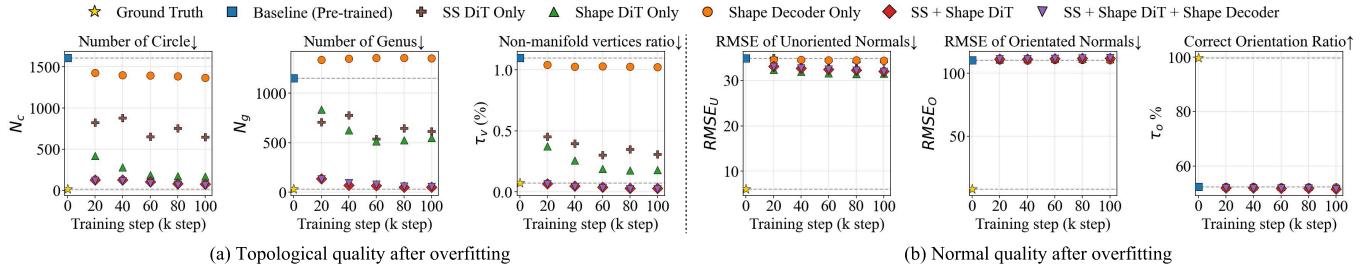


Fig. 3. The topological and normal quality with different training steps of Trellis2 on open surface data. SS DiT is the Sparse Structure DiT.

stabilizing the optimization. Given the solved dual vertices and edge intersection flags, conversion is efficient and bidirectional: mesh  $\rightarrow$  O-Voxel (FDG) computes Hermite data and solves Eq. (1), whereas O-Voxel (FDG)  $\rightarrow$  mesh connects neighboring dual vertices across intersected edges to form quads (then split into triangles).

Beyond the representation, Trellis2 is a large-scale, three-stage 3D-native DiT pipeline pre-trained on 970K 3D assets: sparse structure generation, shape generation, and material generation, built upon VAE and flow-matching DiT paradigm [Esser et al. 2024; Xiang et al. 2025b]. To better understand Trellis2 on open surfaces, we conduct pre-experiments to investigate the following research questions:

- 1) **RQ1**: the boundary of Trellis2 in open surface generation;
- 2) **RQ2**: the underlying cause of persistent normal issues.

### 3.2 What’s Upper Bound on Open Surface Generation?

To establish Trellis2’s upper bound for open surface generation, we deliberately overfit its shape-related components (sparse structure DiT, shape DiT, and shape VAE decoder) on a 500-instance subset of open-surface garments (GarmageSet [Li et al. 2025c]). By factoring out generalization, this setup isolates the model’s inherent capacity ceiling. As shown in Fig. 3, the model clearly learns to represent open surfaces: jointly training all shape components drastically reduces topological errors, with the number of circles ( $N_c$ ) dropping from over 1500 to roughly 100. In contrast, normal-related metrics show zero improvement throughout training. The correct face orientation ratio ( $\tau_o$ ) remains persistently at  $\sim 50\%$ , while the oriented normal RMSE ( $RMSE_O$ ) hovers  $\sim 110^\circ$ .

**Finding 1.** Even under intentional overfitting, the normal metrics (especially orientation) remain far from the ground truth, which is substantially more so than the topology metrics, motivating our next question on why normal issues persist?

### 3.3 Why are Normal Issues Persistent?

The generation quality of DiT is fundamentally bounded by the reconstruction quality of its preceding VAE [Yao et al. 2025; Zheng et al. 2025], which in turn is constrained by whether the 3D representation can faithfully encode the original mesh. Because the DiT is trained to model the latent distribution of the VAE, and the VAE is trained to reconstruct the intermediate 3D representation rather than the raw mesh, any geometric or topological inaccuracies introduced at the representation or VAE stage will inevitably persist and even be amplified during generation.

Motivated by this observation, we skip the DiT stage and focus on the 3D representation and the Shape-VAE reconstruction process.

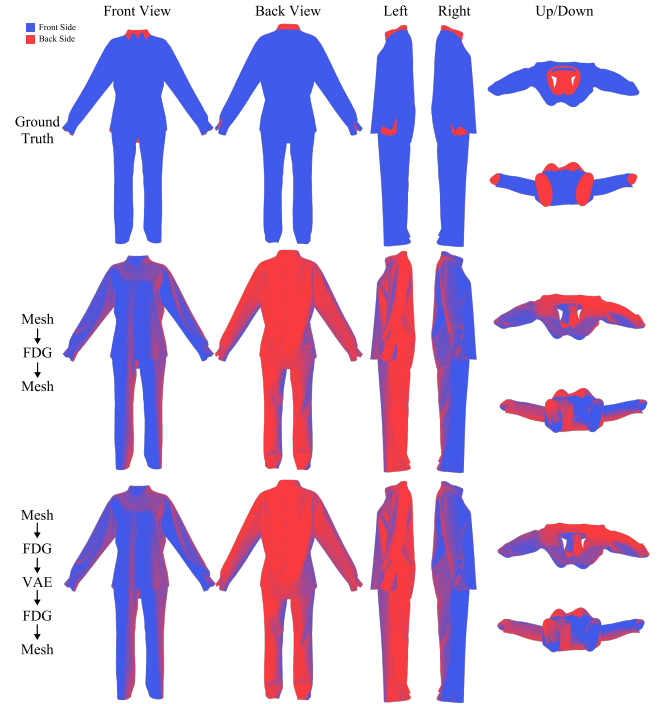


Fig. 4. Incorrect face orientation already emerges in the Flexible Dual Grid (FDG) representation and persists after Shape-VAE reconstruction.

Fig. 4 visualizes the failure mode: in the ground truth (first row), most of the garment is blue (front side), with only small areas such as the collar and cuff being red (back side); but after processing (second and third rows), the garment of back and left view becomes mostly red, with only a small amount of blue remaining at the edges, and the front and back orientations are completely in chaos. Such errors are observed on both open and closed surface.

**Finding 2.** The face orientation becomes unreliable already at the 3D representation, i.e., the Flexible Dual Grid (FDG) stage, and the Shape-VAE reconstruction does not correct this issue.

## 4 Approach

Building on these findings, our goal is to inject correct face orientation into the pipeline while preserving generative priors of base model. To this end, we introduce *FDG-D* (Flexible Dual Grid with Directed Edge, Sec. 4.1), a minimal 3D representation that explicitly

encodes normal direction via directed edges. To learn this representation, we propose *ROS-FT* (Real Open Surface Finetuning, Sec. 4.2), a progressive post-training strategy. To prevent degradation of the original generative priors, we design a lightweight *DE-Adapter* (Directed Edge Adapter, Sec. 4.3)—a parallel Feature Pyramid Network that leverages multi-scale global context to predict edge directions while keeping the base shape decoder frozen. Finally, to better benchmark performance, we construct *Outfit3D* (Sec. 4.4), the first hybrid dataset comprising both open- and closed-surface 3D fashion assets.

#### 4.1 FDG-D

Because the field-free 3D shape representation (FDG) in Trellis2 [Xiang et al. 2025a] discards explicit normals and gradients, face orientation inherently becomes undetermined. Our proposed *FDG-D* resolves this by retaining normal direction from the original mesh, thereby unlocking the true capacity ceiling of Trellis2.

**FDG.** The original *Mesh*→*FDG* extraction entirely ignores normal information. During the *FDG*→*mesh* reconstruction, the winding order of each generated quad (i.e., its face orientation) is deterministically hardcoded based on the coordinate axis ( $x$ ,  $y$ , or  $z$ ) of its corresponding active edge. Because this winding is strictly bound to the spatial axis rather than the actual surface geometry, the algorithm cannot determine the true surface sidedness (front/back). Consequently, the extracted meshes suffer from arbitrary, chaotic face orientations, which is observed across open and closed surfaces.

**FDG-D.** To resolve the winding ambiguity, *Mesh*→*FDG-D* explicitly encodes the direction in which edge pierces the surface. For each active voxel, we store a 3-bit directional data corresponding to how its incident edges along the  $X$ ,  $Y$ , and  $Z$  axes intersect the mesh surface, compactly packed into a single uint8 variable to minimize storage, inspired by intersect flags. To acquire these directions, we propose an *Exact Edge-Ray Intersection* approach: each active dual-grid edge is treated as a ray to perform explicit ray-triangle intersection tests against the ground-truth mesh, yielding the exact direction of the edge as it penetrates the surface at the true intersection point. During the *FDG-D*→*mesh* reconstruction, the algorithm deterministically recovers the correct quad winding from these stored directions, as shown in the fourth step of Fig. 5. When generating a quad corresponding to an active edge, we evaluate whether its default geometric normal aligns with the expected crossing direction ( $d_{\text{expected}} \in \{-1, 1\}$ ) retrieved from the *FDG-D* representation. If the default winding order contradicts the stored edge direction, we dynamically flip the quad’s vertex indices (i.e., swapping the order from  $[v_0, v_1, v_2, v_3]$  to  $[v_0, v_3, v_2, v_1]$ ) prior to triangulation. This lightweight mechanism guarantees that the final reconstructed mesh strictly adheres to the right face orientation.

#### 4.2 ROS-FT Strategy

To unlock true open-surface generation capabilities—producing consistent face orientations—without sacrificing original performance on closed surfaces, we propose *ROS-FT* (Real Open Surface Finetuning). As shown in Fig. 6, *ROS-FT* is designed as a progressive, three-stage post-training pipeline: Stage 1 for DiT alignment, Stage 2 for FDG base reconstruction, and Stage 3 for *DE-Adapter* normal-aware tuning. Crucially, across all stages, we co-train on both open

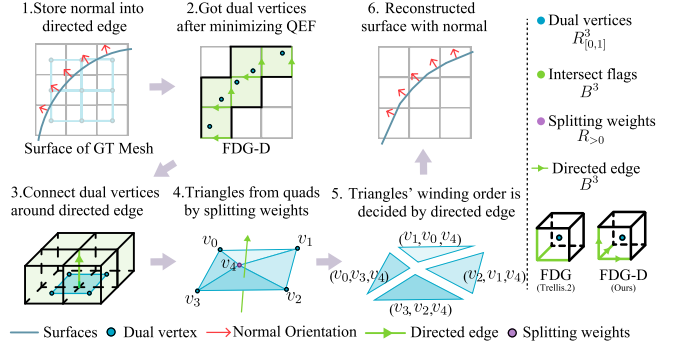


Fig. 5. *FDG-D* (Flexible Dual Grid with Directed Edge) preserves the face orientation from GT Mesh in the directed edge, and uses it to orient the edge during the encoding (mesh → *FDG-D*), then determines the winding order by the edge orientation during the decoding (*FDG-D* → mesh).

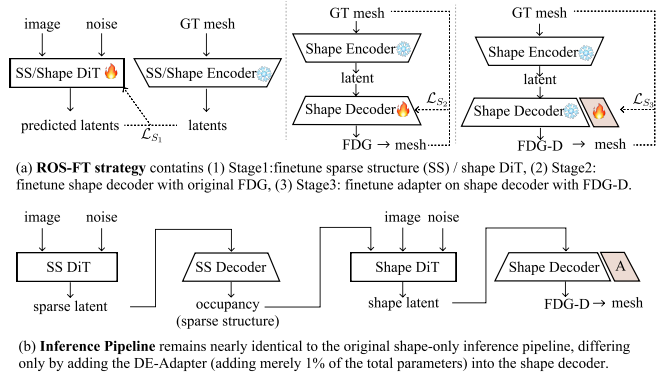


Fig. 6. The (a) training and (b) inference pipeline of our method. A means Directed Edge Adapter (*DE-Adapter*) on shape decoder.

and closed surface data, using the latter as a regularization mechanism to preserve the model’s foundational geometry priors.

**Stage 1: DiT Alignment.** The purpose of this stage is to align the latent generation capability with new data distribution. We finetune the rectified flow models (sparse structure DiT and shape DiT) using original forward process and optimize the neural network  $v_\theta$  via standard conditional flow matching (CFM) loss [Lipman et al. 2023]:

$$\mathcal{L}_{S1} = \mathbb{E}_{t, x_0, \epsilon} \|v_\theta(x, t) - (\epsilon - x_0)\|_2^2. \quad (2)$$

**Stage 2: FDG Base Reconstruction.** This stage aims to establish a robust foundation for decoding latents into explicit 3D geometry using the vanilla FDG representation. To strictly preserve the generative priors and avoid disrupting the latent space matched by the DiT pipeline, we keep the Shape VAE encoder completely frozen and solely fine-tune the decoder. The decoder is optimized using the original reconstruction objective  $\mathcal{L}_{S2}$ , which comprises structural, geometric, and rendering-based perceptual losses:

$$\mathcal{L}_{S2} = \lambda_v |\hat{v} - v|_2^2 + \lambda_\delta \text{BCE}(\hat{\delta}, \delta) + \lambda_\rho \text{BCE}(\hat{\rho}, \rho) + \lambda_{\text{KL}} \mathcal{L}_{\text{KL}} + \mathcal{L}_{\text{render}}. \quad (3)$$

Methods	Surface Type	Texture	Multi-items
GarmentCode [ECCV 24]	open surface (garment only)	✗	✗
GarVerseLOD [TOG 24]	open surface (garment only)	✗	✗
GarmageSet [TOG 25]	open surface (garment only)	✗	✗
Outfit3D (Ours)	hybrid surface (outfits)	✓	✓

Table 2. Differences with existing garment modeling datasets.

**Stage 3: DE-Adapter Tuning.** As the core of our strategy, Stage 3 addresses the critical orientation ambiguity inherent in the vanilla FDG. By the end of Stage 2, the Shape VAE has already been heavily constrained by 7 complex losses and predicts a 7-dimensional geometric output (including splitting weights for quad topology) based on a 6-dimensional input (dual vertices and intersected flags, as shown in Fig. 5). Introducing a new, explicit normal-orientation target directly into this base network severely destabilizes its pre-trained topological capabilities—an optimization conflict we empirically verify in our ablation studies (see Tab. 6 (c) and (d)).

To avoid this conflict and safely inject face orientation information without compromising the original Shape VAE’s performance, Stage 3 introduces a lightweight Directed Edge Adapter (*DE-Adapter*) branch alongside the strictly frozen base decoder. This adapter is tasked exclusively with predicting the crossing direction (the green vector in the 4th step of Fig. 5) logits  $\hat{c} \in \mathbb{B}^3$  for each spatial axis. To ensure the model focuses solely on valid geometry, the crossing direction loss is computed exclusively on the active voxels where the ground-truth intersection flag  $\delta$  is True. The supervision is formulated as a Binary Cross-Entropy with Logits loss against the ground-truth crossing direction  $c \in \{0, 1\}^3$ :

$$\mathcal{L}_{s3} = \lambda_{s2} \mathcal{L}_{s2} + \lambda_{cd} \cdot \text{BCE}(\hat{c}_{[\delta=1]}, c_{[\delta=1]}) \quad (4)$$

where  $\lambda_{s2}$  and  $\lambda_{cd}$  are weights of stage 2 loss and crossing direction loss, respectively. By restricting the trainable parameters to the adapter branch, Stage 3 effectively equips the decoder with precise face orientation awareness at a minimal computational cost.

### 4.3 DE-Adapter

To preserve the priors acquired during pre-training, our DE-Adapter (Directed Edge Adapter) is designed as a parallel Feature Pyramid Network (FPN) alongside the frozen shape decoder. Inspired by successful adapters in image generation [Shi et al. 2026, 2025; Ye et al. 2023; Zhang et al. 2023a], this architecture allows the model to predict crossing edge directions without interfering with the base network. Predicting the correct direction fundamentally requires global context to determine the true surface sidedness (front/back), particularly in complex self-occlusion regions or thin garments. Therefore, the adapter extracts and processes intermediate features at every resolution stage from the shape decoder, fusing them with its own hidden state before upsampling. Crucially, it reuses the spatial subdivision topology (subdiv) predicted by the base branch, ensuring the spatial alignment. This progressive, multi-scale integration grants the orientation prediction a global receptive field, significantly boosting the raw face orientation accuracy for complex open surfaces while maintaining parameter efficiency.

### 4.4 Outfit3D Dataset

Previous garment modeling datasets [Korosteleva et al. 2024; Luo et al. 2024; Zou et al. 2023] primarily focus on isolated, open-surface garments. As summarized in Tab. 2, they lack the multi-item complexity inherent to real-world outfits. To bridge this gap and push the field toward realistic, production-level fashion generation, we construct *Outfit3D*. As shown in Fig. 7, this dataset provides complex, multi-item outfits that combine both open- and closed-surface components, complete with high-resolution textures.

*Data Collection and Processing Pipeline.* The raw 3D assets in our dataset are sourced from open-source design communities and commercially purchased models, encompassing both standalone cloth assets and fully clothed human models. To ensure high-quality, production-ready geometry, we developed a rigorous three-step data curation pipeline: (1) *Garment Standardization via CLO3D*: Using the professional apparel design software CLO3D, we first standardize the UV layouts and bake all Physically Based Rendering (PBR) texture channels. The garments are then exported as high-fidelity thin-shell (open surface) meshes. (2) *Artifact Removal*: We utilize Blender scripts to automatically detect and delete non-garment auxiliary meshes from the exported models, such as transparent collision-bounding boxes for shoes and transparent simulation-assist patches on the garments. (3) *Avatar Removal and Export*: Finally, we strip the underlying human body meshes while preserving essential closed surface accessories (e.g., shoes, belts, and bags), exporting the finalized hybrid surface meshes for training. Further details of dataset statistics are provided in the supplementary material.

## 5 Experiments

### 5.1 Implementation Details

*Training Configurations.* All experiments are conducted on  $2 \times \text{H200}$  (141 GiB) GPUs. The ROS-FT strategy is executed sequentially. In Stage 1, we finetune the sparse structure DiT and the shape DiT following the original settings, utilizing a batch size of 24 with learning rates of  $1 \times 10^{-4}$  and  $2 \times 10^{-5}$ , respectively, using the AdamW optimizer. In Stage 2, we freeze the shape encoder and finetune the shape decoder using a batch size of 48 and a learning rate of  $1 \times 10^{-5}$ . Finally, in Stage 3, we freeze the entire base VAE and train the proposed DE-Adapter with a learning rate of  $1 \times 10^{-3}$ .

*Dataset Setup.* To construct a comprehensive training and evaluation benchmark, we compile a mixed dataset containing 10,489 assets. This collection comprises 3,724 single-item open surface garments from GarmageSet [Li et al. 2025c], 3,266 outfits from our proposed Outfit3D dataset, and 3,499 closed surface objects from ObjaverseXL [Deitke et al. 2023a]. The inclusion of the ObjaverseXL data acts as a regularization mechanism to preserve the pre-trained model’s general 3D generation capabilities. From each of these three domains, we randomly reserve 100 assets (300 in total) for evaluation, leaving the remaining 10,189 assets for training.

*Ablation and Inference Settings.* To accelerate experimental iterations under limited computing resources, our ablation studies regarding FDG-D representation (for Shape VAE reconstruction and shape generation, i.e., Tab. 6 and Tab. 7) are conducted on a lightweight subset. We randomly sample 500 assets from GarmageSet [Li et al. 2025c] for training and another 50 for evaluation. Furthermore,



Fig. 7. Examples of Outfit3D, GarmageSet, and GarVerseLOD.

for quantitative evaluation in shape generation, we deliberately disable post-processing steps (such as remeshing) from the original Trellis2 inference pipeline, retaining only hole-filling. This ensures that the reported metrics strictly reflect the original normal quality of the generated mesh without external refinement.

## 5.2 Evaluation Metrics

**Geometry Accuracy.** To comprehensively evaluate geometric fidelity, we employ three standard metrics following established protocols [Lin et al. [n. d.]; Yang et al. 2025b]. First, Chamfer Distance (CD) is used to measure the bidirectional point-to-point surface deviation between the generated meshes and the ground truth by uniformly sampling  $10^5$  points on the surfaces. Second, we report the F-Score at a specified distance threshold ( $\tau = 0.03$  m) to evaluate the percentage of correctly reconstructed surfaces, capturing both precision and recall. Finally, Voxel IoU (Intersection over Union) is computed on a rasterized  $64^3$  grid to assess the global structural preservation.

**Normal Quality.** Face orientation is a critical focus of our work. Following NeuralGF [Li et al. 2023a], we report two Root Mean Square Error (RMSE) metrics between the ground-truth normals  $\hat{\mathbf{n}}_i$  and the estimated normals  $\mathbf{n}_i$ : the unoriented error  $RMSE_U = \sqrt{\frac{1}{I} \sum_{i=1}^I (\arccos(|\hat{\mathbf{n}}_i \odot \mathbf{n}_i|))}$  and the oriented error  $RMSE_O = \sqrt{\frac{1}{I} \sum_{i=1}^I (\arccos(\hat{\mathbf{n}}_i \odot \mathbf{n}_i))^2}$ . Here,  $RMSE_U \in [0^\circ, 90^\circ]$  and  $RMSE_O \in [0^\circ, 180^\circ]$ ;  $I$  is the number of evaluated normals ( $10^4$  points sampled on the prediction mesh queried against the nearest ground-truth triangles),  $\odot$  denotes the inner product, and  $|\cdot|$  denotes the absolute value. Crucially, we also report the orientation error rate  $\tau_o(\%)$ , computed as  $100 - \text{Correct orientation}(\%)$ . A lower  $\tau_o$  indicates better inside-outside differentiation, allowing a global flip of predicted normals if it yields a lower error to account for global ambiguity.

**Topology Quality.** We follow DoubleCoverUDF [Hou et al. 2023] to assess topological robustness by percentage of non-manifold vertices  $\tau_v(\%)$ , the number of boundary edges  $N_b$ , the number of open edge circles (boundary loops)  $N_c$ , and the genus  $N_g$ . Non-manifold vertices occur when local neighborhoods intersect at a single point (forming multiple topological disks), which we conservatively identify via edges shared by more than two triangles. These defects are highly undesirable as they destabilize downstream simulations, and forcefully removing them often introduces unwanted holes.  $N_b$ ,

$N_c$ , and  $N_g$  capture the global topological features. The genus  $N_g$  is derived directly from the Euler characteristic of generated mesh.

## 5.3 Comparison

We comprehensively evaluate our approach across three domains: pure open, pure closed, and hybrid surfaces. We first compare against garment-specific baselines (ChatGarment [Bian et al. 2025], Design2GarmentCode [Zhou et al. 2025], and SewingLDM [Liu et al. 2025]), which synthesize meshes by predicting 2D patterns and stitching them via physical simulation. Because these methods cannot generate pure closed surfaces, we test them only on GarmageSet and Outfit3D datasets. Furthermore, while their pattern-stitching paradigm inherently prevents non-manifold vertices and genus artifacts (making direct topology comparisons inapplicable), it introduces severe simulation bottlenecks: on our evaluation set, SewingLDM only simulated 28 cases successfully, and Design2GarmentCode failed on 2 cases. In contrast, our AnySurf pipeline directly generates any surface with a 100% success rate.

**5.3.1 Quantitative Comparison. Performance on open surfaces.** We first evaluate the models on the open surface domain (GarmageSet) (Tab. 3). While garment-specific models (ChatGarment, Design2GarmentCode, SewingLDM) are natively designed for this domain, their pattern-stitching paradigm struggles to accurately reconstruct complex 3D shapes, resulting in lower geometric fidelity (e.g., lower F-Score and Voxel IoU) and poor face orientation ( $\tau_o \approx 84 - 85\%$ ). Compared to general 3D generators, the original Trellis2 baseline exhibits catastrophic normal flipping ( $\tau_o = 52.29\%$ ) and severe topological defects (over 1900 open edge circles). Directly fine-tuning Trellis2 significantly improves geometry but fundamentally fails to resolve the normal ambiguity ( $\tau_o = 51.71\%$ ). In contrast, our full AnySurf pipeline rectifies this deficiency, achieving state-of-the-art normal quality ( $\tau_o = 90.39\%$ ) while preserving the highest geometric accuracy ( $IoU = 0.7674$ ) and topological robustness.

**Performance on hybrid surfaces.** We further extend our evaluation to the more challenging hybrid surface from our Outfit3D dataset. Outfit3D presents significantly higher topological complexity than GarmageSet: intricate structures like lace and complex seams (Fig. 7) surge its average GT open boundary circles ( $N_c$ ) to 2512.7, compared to GarmageSet's 16.9. As shown in Tab. 4, the presence of mixed

open and closed topologies exposes the limitations of existing methods. Garment-specific baselines suffer a severe performance drop when forced to handle hybrid structures (e.g., outfits containing solid shoes or thick belts). Their geometric fidelity degrades significantly (IoU drops to  $\approx 0.12 - 0.15$ , and CD surges to  $\approx 0.13 - 0.17$ , an order of magnitude higher than ours), confirming that 2D sewing-pattern paradigms cannot generalize to real-world outfits with closed volumetric components. On the other hand, the general-purpose Trellis2 baseline maintains decent geometric accuracy but completely fails to differentiate the front side from the back side ( $\tau_o = 52.82\%$ ). While fine-tuning Trellis2 on hybrid data improves geometric alignment (IoU = 0.7220), it remains blind to orientation ( $\tau_o = 52.31\%$ ). Ours successfully bridges this gap and achieves the best normal quality ( $\tau_o = 86.21\%$ ) and the lowest oriented error (RMSE<sub>O</sub> = 57.035°), while simultaneously delivering the highest geometric accuracy (CD = 0.0164) and robust topology ( $\tau_v = 1.3607\%$ ).

**5.3.2 Qualitative Comparison.** SewingLDM does not support rendered image conditioning; we therefore use its sketch-based input for that model and rendered images for all other methods under otherwise identical evaluation settings. Fig. 8 shows qualitative results on *open surfaces* (GarmageSet). Garment-specific baselines (ChatGarment, Design2GarmentCode, and SewingLDM) mostly preserve coherent inside-outside shading (blue exteriors and red interiors), but their sewing-pattern pipelines cap geometric complexity and yield overly simplified shapes. The general-purpose Trellis2 baseline instead produces fragmented meshes and severe normal noise, with red and blue interleaved on outward-facing regions. Fine-tuning Trellis2 improves geometric fidelity yet leaves orientation largely unresolved. In contrast, our method recovers intricate wrinkles and folds and attains clean, globally consistent face orientations that closely align with the ground truth.

**Performance on hybrid surfaces.** We further compare visual quality on the more challenging Outfit3D dataset (Fig. 9), which mixes open (e.g., dresses) and closed (e.g., shoes) topologies. Garment-specific baselines struggle significantly here: they completely fail to generate closed components like shoes, and their outputs for the main garments are overly simplistic, lacking the fidelity to align with the input images. While the general-purpose Trellis2 can generate all components, it produces severely corrupted geometries and chaotic normals, with large patches of red incorrectly appearing on the exterior of both garments and shoes. Fine-tuning Trellis2 improves structural coherence, but the normal flipping issue persists, particularly on complex regions and closed structures. In contrast, our method robustly handles hybrid topologies, generating highly detailed geometries for both open garments and closed accessories while consistently maintaining correct face orientations across all components, achieving results align with the ground truth.

**Performance on closed surfaces.** Fig. 10 shows closed surface examples (e.g., characters, vehicles); garment-specific baselines do not apply, so we compare only to Trellis2 and its finetuned variant. Both still exhibit red-blue interleaving artifacts remains unreliable even on watertight meshes. AnySurf outperforms them with coherent orientation (uniform blue) without degrading shape fidelity.

## 5.4 Ablation Study

**5.4.1 Ablation of FDG-D.** On the **3D representation reconstruction** task (mesh  $\rightarrow$  FDG-D  $\rightarrow$  mesh), we evaluate the intrinsic fidelity of the representation itself without any neural network intervention. We use 300 instances in total, with 100 drawn from each of GarmageSet [Li et al. 2025c], Objaverse-XL [Deitke et al. 2023b], and our Outfit3D dataset. The quantitative results are reported in Tab. 5. The baseline FDG suffers from severe normal flipping ( $\tau_o \approx 51.62\%$ , near random guessing) due to the lack of explicit orientation encoding, which visually manifests as chaotic red/blue surface patches (see Fig. 11). To address this, we ablate two variants of normal assignment for our FDG-D representation: (a) *Voxel Normal Guidance*, which computes and stores the average normal of all surfaces intersecting a voxel; and (b) *Ray Intersection*, which explicitly stores the exact crossing direction of the active edges based on explicit ray-triangle intersection tests against the ground-truth mesh. As shown in Tab. 5 and qualitatively corroborated in Fig. 11, voxel-level averaging yields only marginal improvements. In contrast, storing the exact edge-ray intersection directions explicitly binds orientation to the topology, significantly boosting the correct orientation rate  $\tau_o$  to 95.04% and drastically reducing the oriented error (RMSE<sub>O</sub>) from 121.7 to 31.7, successfully restoring uniform, ground-truth-level normals across open, closed, and hybrid surfaces, all without compromising geometry or topology accuracy.

On the **shape VAE reconstruction** task (mesh  $\rightarrow$  FDG-D  $\rightarrow$  Shape VAE  $\rightarrow$  FDG-D  $\rightarrow$  mesh), to accelerate experimental iterations under limited computing resources, we only use 500 instances from GarmageSet [Li et al. 2025c]. And we train the Shape VAE decoder while freezing the encoder for keeping the latent space as same as DiT. The quantitative results are reported in Tab. 6. To systematically validate our DE-Adapter design, we perform extensive ablations on the network architecture and training strategies. First, we investigate the source of edge direction during the decoding phase (FDG-D  $\rightarrow$  mesh). As shown in variants (c) and (d), using ground-truth orientations (d) instead of predicted ones (c) yields similar performance. However, to maintain consistency with the topological splitting weights (which rely on ground truth during decoding), we adopt GT orientations for subsequent ablations. Second, we demonstrate that directly fine-tuning the base decoder on the FDG-D representation (variants c, d, g) successfully improves normal quality but inevitably degrades the topology quality (e.g.,  $N_c$  and  $N_g$  significantly increase compared to the baseline). Third, we evaluate the addition of a simple linear head (variants e, f). While this two-stage approach preserves the pretrained topology, the shallow head lacks the capacity to learn complex edge directions even with maximum loss weights, resulting in a low  $\tau_o$  of 58.93%. Finally, our introduced DE-Adapter (variant h, with  $\mathcal{L}_{s2} = 0$ ) resolves this dilemma. The model successfully learns the correct face orientation ( $\tau_o = 90.67\%$  at depth 32) while strictly guaranteeing that the topological quality remains completely unaffected compared to the finetuned baseline. Notably, increasing the complexity of the adapter (scaling the depth from 8 to 32) enhances normal quality without compromising either geometric accuracy or topology quality. Furthermore, Fig. 12 reveals that while the VAE fails to capture normal directionality using the original FDG, our FDG-D representation effectively enables the model to acquire this capability.

Methods	Geometry Accuracy			Normal Quality			Topology Quality		
	CD↓	F-Score↑	IoU↑	$RMSE_U$ ↓	$RMSE_O$ ↓	$\tau_o$ (%)↑	$N_c$ ↓	$N_g$ ↓	$\tau_v$ (%)↓
Ground Truth	0.003557	1.0000	1.0000	6.021	7.953	99.80	16.9	29.4	0.0036
ChatGarment	0.058705	0.9620	0.3147	42.351	59.520	85.24	-	-	-
Design2GarmentCode	0.049524	0.9703	0.3703	43.587	61.039	84.44	-	-	-
SewingLDM	0.072085	0.9483	0.2496	46.007	60.607	84.67	-	-	-
Trellis2	0.024585	0.9287	0.5842	33.868	109.798	52.29	1909.1	1325.6	1.9782
Trellis2 (Finetuned)	<b>0.012772</b>	<b>0.9904</b>	<b>0.7674</b>	23.533	115.530	51.71	122.9	23.4	0.1801
Ours	0.012774	<b>0.9904</b>	<b>0.7674</b>	<b>21.679</b>	<b>48.112</b>	<b>90.39</b>	<b>121.2</b>	<b>21.8</b>	<b>0.1771</b>

Table 3. Quantitative comparison of our method with state-of-the-art models on pure open surface (GarmageSet) generation task.

Methods	Geometry Accuracy			Normal Quality			Topology Quality		
	CD↓	F-Score↑	IoU↑	$RMSE_U$ ↓	$RMSE_O$ ↓	$\tau_o$ (%)↑	$N_c$ ↓	$N_g$ ↓	$\tau_v$ (%)↓
Ground Truth	0.002929	1.0000	1.0000	13.371	24.576	97.53	2512.7	9.3	2.4926
ChatGarment	0.136093	0.7725	0.1436	46.220	63.220	82.70	-	-	-
Design2GarmentCode	0.142790	0.7436	0.1509	46.412	64.635	81.31	-	-	-
SewingLDM	0.176955	0.6040	0.1244	45.945	63.385	84.13	-	-	-
Trellis2	0.023919	0.9354	0.6194	36.700	108.241	52.82	2132.6	2298.0	2.8546
Trellis2 (Finetuned)	0.017087	<b>0.9672</b>	0.7220	32.572	110.986	52.31	781.8	110.7	1.3609
Ours	<b>0.016433</b>	<b>0.9672</b>	<b>0.7309</b>	<b>29.645</b>	<b>57.035</b>	<b>86.21</b>	<b>781.7</b>	<b>109.0</b>	<b>1.3607</b>

Table 4. Quantitative comparison of our method with state-of-the-art models on hybrid surface data (Outfit3D) generation task.

Methods	Geometry Accuracy			Normal Quality			Topology Quality		
	CD↓	F-Score↑	IoU↑	$RMSE_U$ ↓	$RMSE_O$ ↓	$\tau_o$ (%)↑	$N_c$ ↓	$N_g$ ↓	$\tau_v$ (%)↓
Ground Truth	0.003588	1.000	1.000	12.574	22.901	96.88	854.3	13.2	1.4328
FDG (Baseline)	0.003614	0.999	0.964	14.221	121.734	51.62	988.6	192.6	2.8959
FDG-D (a)	0.003613	0.999	0.964	14.215	106.353	62.19	988.7	192.6	2.8958
FDG-D (b)	0.003614	0.999	0.964	14.192	31.775	95.04	988.6	192.6	2.8958

Table 5. Ablation study of FDG-D on 3D representation reconstruction with different settings: (a) use voxel normal guidance and (b) use edge-ray intersection.

**5.4.2 Ablation of DE-Adapter.** Tab. 7 reports the full **shape generation** pipeline (Image  $\rightarrow$  DiTs  $\rightarrow$  Shape VAE  $\rightarrow$  FDG-D  $\rightarrow$  Mesh). While DE-Adapter v1 (a simple MLPs architecture acting only on the final stage) improves normal quality over the finetuned baseline without hurting geometry or topology, its  $\tau_o$  drops from 90.67% in pure VAE reconstruction (Tab. 6) to 87.55% in the full 512-resolution DiT generation pipeline. We attribute this performance gap to the noisy latents produced by DiT and the resulting domain shift from ground-truth latents. This issue is further compounded because v1 operates exclusively at the final high-resolution (1 $\times$ ) stage, limiting its receptive field to local features. To address this, DE-Adapter v2 introduces a Feature Pyramid Network (FPN) architecture that fuses features across all five decoding stages (16 $\times$  to 1 $\times$ ) by reusing the shape decoder’s subdivision topology. This restores global context, successfully raising  $\tau_o$  to 91.44% and reducing  $RMSE_O$  to 46.3° while keeping the topology almost unchanged. Furthermore, our DE-Adapter design remains resolution-agnostic: the v2 adapter

trained purely at 512 resolution can be directly applied to the 1024-resolution generation pipeline (Tab. 7, bottom) without any extra fine-tuning, still yielding a robust  $\tau_o$  of 85.94%.

**5.4.3 Ablation of ROS-FT.** To comprehensively evaluate the contributions of individual training modules within our ROS-FT pipeline, we conduct an ablation study using the full 10K mixed 3D assets dataset (comprising open, closed, and hybrid surfaces). The quantitative results on the evaluation set are presented in Tab. 8. Starting from the pretrained Trellis2 baseline, sequentially fine-tuning the Sparse Structure DiT (+A), Shape DiT (+B), and Shape Decoder (+C) on our dataset leads to progressive improvements in both Geometry Accuracy (e.g., F-Score rises from 0.8515 to 0.8831) and Topology Quality (e.g., non-manifold vertices  $\tau_v$  drop from 1.86% to 0.77%). However, fine-tuning these base modules alone (even when combined as +A & B & C) fails to resolve the inherent normal flipping issue, with the correct orientation rate ( $\tau_o$ ) persistently remaining around 53%. It is only with the introduction of our final training

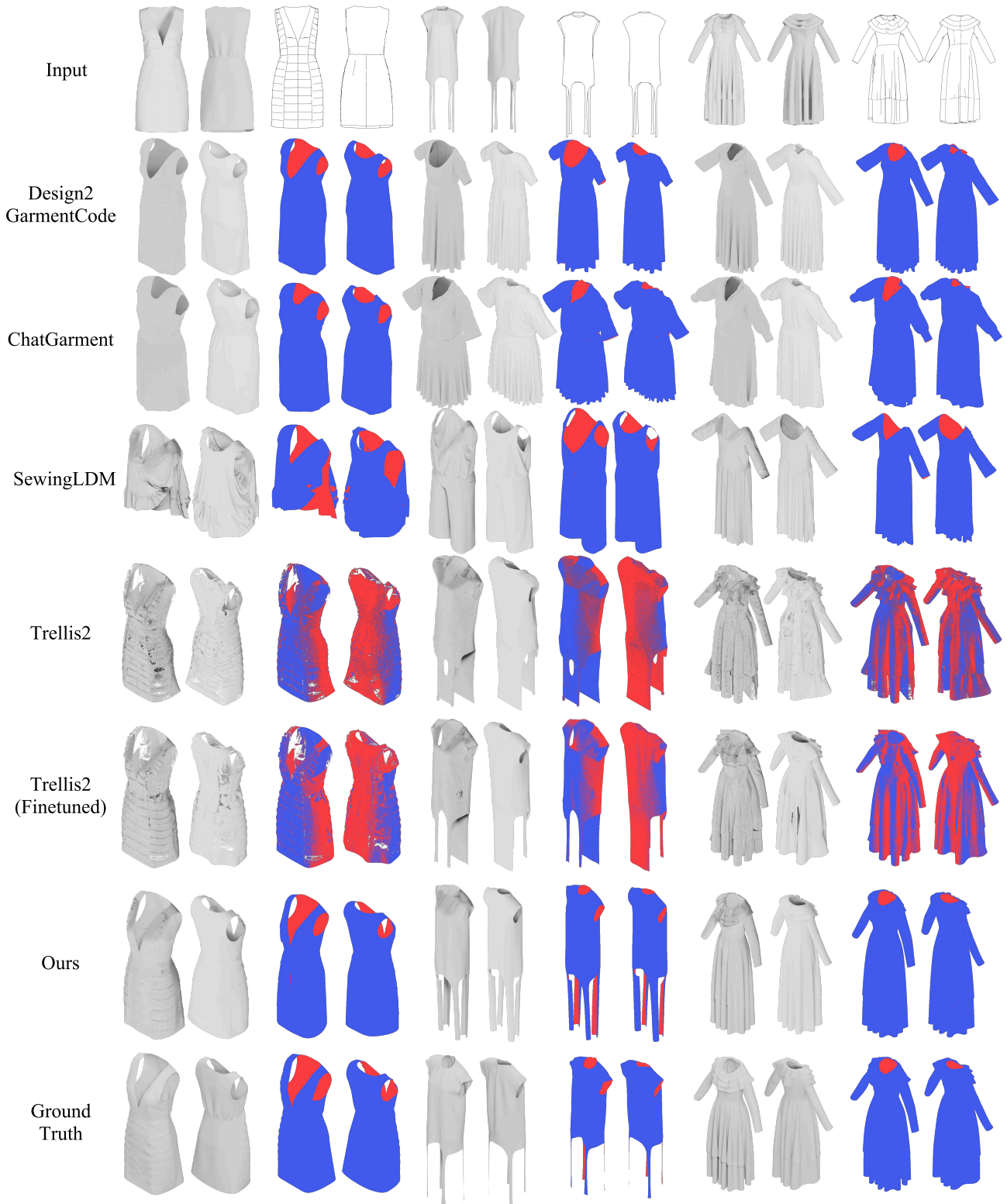


Fig. 8. Qualitative comparison on pure open surface (GarmageSet) generation task.

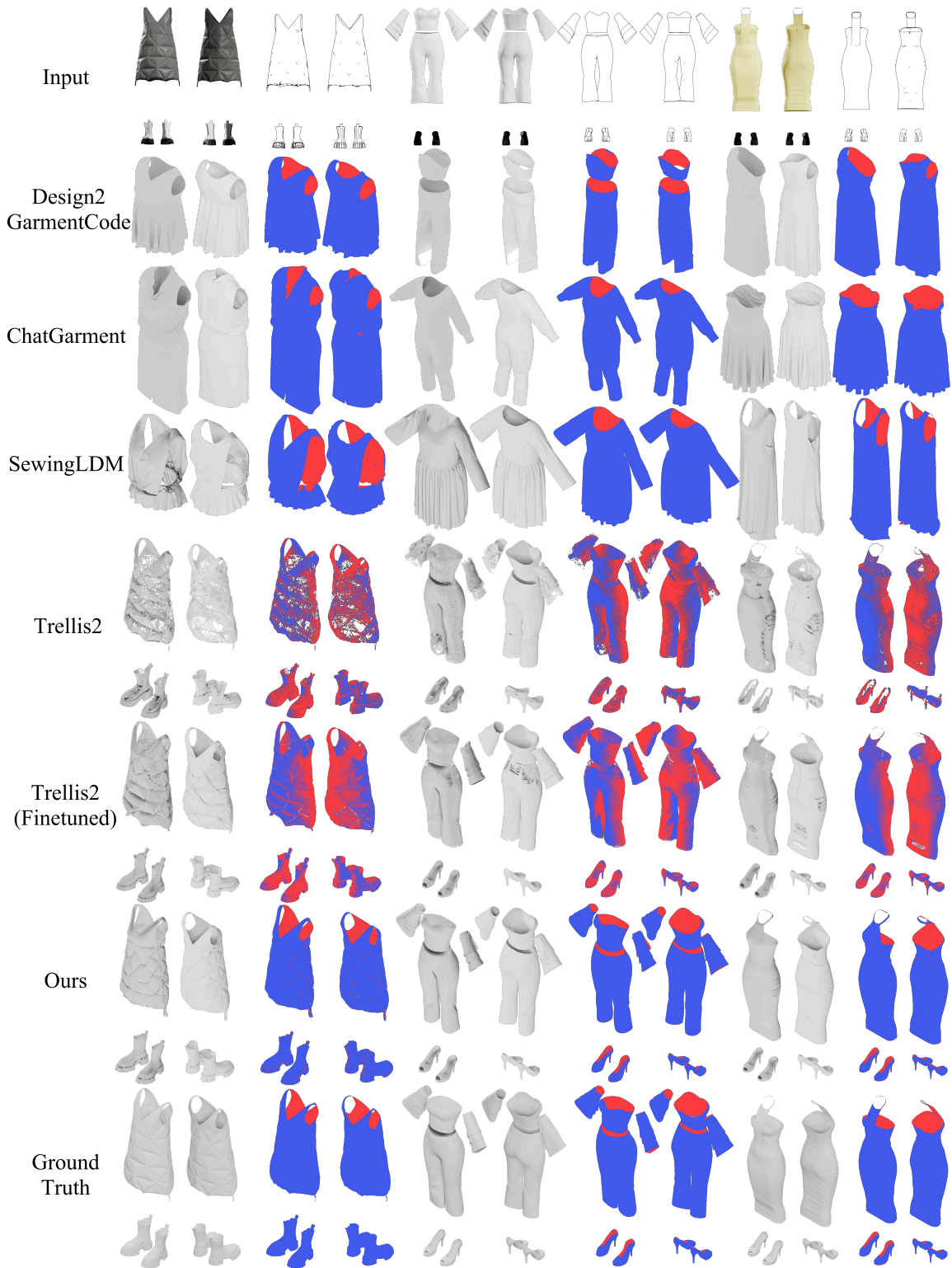


Fig. 9. Qualitative comparison on hybrid data (Outfit3D) generation task.

Methods	Geometry Accuracy			Normal Quality			Topology Quality		
	CD↓	F-Score↑	IoU↑	$RMSE_U$ ↓	$RMSE_O$ ↓	$\tau_o$ (%)↑	$N_c$ ↓	$N_g$ ↓	$\tau_v$ (%)↓
Ground Truth	0.003584	1.000	1.000	6.017	7.980	99.77	17.8	32.4	0.0038
Pretrained decoder + FDG	0.003588	1.000	0.9698	6.543	122.286	52.20	707.9	121.9	0.6805
Finetuned decoder + FDG (Baseline)	0.003588	1.000	0.9695	6.373	122.230	52.22	718.8	190.5	0.6128
Finetuned decoder + FDG-D (c)-0.1	0.003591	1.000	0.9698	7.274	20.558	97.75	1050.7	240.1	1.0397
Finetuned decoder + FDG-D (d)-0.1	0.003592	1.000	0.9698	7.209	20.154	97.88	1052.6	238.8	1.0409
Finetuned decoder + FDG-D (d)-0.05	0.003594	1.000	0.9697	7.215	22.302	97.46	1035.3	235.6	1.0387
Finetuned decoder + FDG-D (d)-0.01	0.003594	1.000	0.9696	7.165	35.962	94.90	999.7	242.0	1.0066
Finetuned decoder + FDG-D (e)-0.01	0.003588	1.000	0.9695	6.381	113.380	58.83	718.8	190.5	0.6128
Finetuned decoder + FDG-D (f)	0.003587	1.000	0.9695	6.400	113.231	58.93	718.8	190.5	0.6128
Finetuned decoder + FDG-D (g)-0.01	0.003592	1.000	0.9686	9.124	30.897	95.94	812.9	220.6	0.6833
Finetuned decoder + FDG-D (h)-8	0.003587	1.000	0.9695	6.360	63.713	86.22	718.7	190.3	0.6128
Finetuned decoder + FDG-D (h)-32	0.003585	1.000	0.9695	6.395	51.016	90.67	718.7	190.3	0.6128

Table 6. Ablation of FDG-D on Shape VAE reconstruction. **Edge-orientation source during decoding:** (c) predicted orientations from the shape decoder; (d) ground-truth orientations from the mesh. **Two-stage training for decoder (stage 2→stage 3):** (e)/(f) only the added edge-orientation head is updated in stage 3; (g) both the new head and full decoder are updated in stage 2&3; (h) the added adapter is updated in stage 3. **Loss:** (c), (d), (e), and (g) use the original loss  $\mathcal{L}_{s2}$  plus  $\mathcal{L}_{cd}$ ; (f)/(h) uses  $\mathcal{L}_{cd}$  only. The weight  $\lambda_{cd}$  of  $\mathcal{L}_{cd}$ : (c)  $\lambda_{cd}=0.1$ ; (d)  $\lambda_{cd} \in \{0.1, 0.05, 0.01\}$ ; (e)-(g)  $\lambda_{cd}=0.01$ . (h)-8/32: depth of adapter( $v1$ )=8/32.

Methods	Geometry Accuracy			Normal Quality			Topology Quality		
	CD↓	F-Score↑	IoU↑	$RMSE_U$ ↓	$RMSE_O$ ↓	$\tau_o$ (%)↑	$N_c$ ↓	$N_g$ ↓	$\tau_v$ (%)↓
Ground Truth	0.003584	1.000	1.000	6.017	7.980	99.77	17.8	32.4	0.0038
<i>SS DiT/Shape DiT 512 + Shape VAE 512</i>									
Pretrained pipeline	0.031009	0.8937	0.5501	35.443	110.330	51.95	2803.8	100.7	11.3697
Finetuned pipeline	0.045229	0.7616	0.3734	32.824	110.976	52.34	219.1	18.3	1.0238
Finetuned pipeline + DE-Adapter v1	0.045209	0.7617	0.3734	32.799	55.146	87.55	219.5	19.4	1.0241
Finetuned pipeline + DE-Adapter v2	0.045206	0.7619	0.3734	32.783	46.344	91.44	219.0	18.3	1.0237
<i>SS DiT/Shape DiT 1024 + Shape VAE 512</i>									
Pretrained pipeline	0.030375	0.8959	0.5599	33.869	110.202	52.53	1724.9	1075.0	1.7782
Finetuned pipeline	0.040729	0.8253	0.4217	31.713	111.869	51.91	137.9	165.1	0.2129
Finetuned pipeline + DE-Adapter v1	0.040751	0.8253	0.4216	31.746	80.133	75.12	138.5	167.3	0.2117
Finetuned pipeline + DE-Adapter v2	0.040749	0.8253	0.4218	31.762	58.801	85.94	138.0	167.4	0.2143

Table 7. Ablation study of DE-Adapter on shape generation under varying DiT resolutions and DE-Adapter architectures.

stage—the FDG-D finetuned DE-Adapter (+D)—that the pipeline successfully overcomes this bottleneck. As shown in the final row (+A & B & C & D), the addition of the adapter dramatically boosts  $\tau_o$  to 81.48% and slashes the  $RMSE_O$  error by nearly half (from 109.7 to 63.348), while strictly preserving the geometric and topological gains achieved in the earlier stages. This result firmly validates the effectiveness of our sequential training strategy and demonstrates that the DE-Adapter is a highly robust solution capable of restoring reliable face orientations across diverse surface types (open, closed, and hybrid) without compromising the priors from pre-training.

## 6 Application and Discussion

### 6.1 Texturing Pipeline Compatibility

The original textured mesh generation in Trellis2 necessitates a post-processing remeshing stage, where the decoded open surface

is converted into a narrow-band Unsigned Distance Function (UDF) and subsequently reconstructed via dual contouring. This procedure ensures consistent face orientations for texture baking, but it introduces topological distortions by closing open boundaries. This effect is evidenced in the rightmost columns of Fig. 13, where only the front-facing (blue) orientations. In contrast, our pipeline generates high-fidelity, globally consistent normals directly, allowing us to bypass this destructive remeshing step. By eliminating the need for UDF-based reconstruction, we facilitate a seamless transition to downstream texturing while strictly preserving the intended open-surface topology of the generated 3D assets.

### 6.2 Multi-item Generation Pipeline

Because our AnySurf pipeline is inherently designed as a unified, one-for-any surface generator, it can seamlessly harness the advanced image generation models like Flux.2 [klein] [Black Forest

Methods	Geometry Accuracy			Normal Quality			Topology Quality		
	CD↓	F-Score↑	IoU↑	RMSE <sub>U</sub> ↓	RMSE <sub>O</sub> ↓	$\tau_o$ (%)↑	$N_c$ ↓	$N_g$ ↓	$\tau_o$ (%)↓
Ground Truth	0.004000	1.0000	1.0000	12.574	22.901	96.88	854.3	13.2	1.4328
Trellis2	0.042809	0.8515	0.5726	39.570	106.540	53.54	1564.9	1574.6	1.8692
+ SS DiT (A)	0.036696	0.8835	0.6726	35.884	109.025	53.19	924.3	998.8	1.2513
+ Shape DiT (B)	0.036668	0.8832	0.6729	34.728	109.644	53.11	574.2	736.2	0.8425
+ Shape Dec. (C)	0.036676	0.8831	0.6729	34.597	109.776	53.06	518.4	727.1	0.7678
+ A & B	0.036683	0.8831	0.6729	34.599	109.719	53.06	520.0	727.7	0.7679
+ A & C	0.036682	0.8831	0.6728	34.627	109.771	53.02	519.8	727.5	0.7682
+ B & C	0.036682	0.8831	0.6728	34.589	109.709	53.07	519.3	728.9	0.7671
+ A & B & C	0.036691	0.8831	0.6729	34.623	109.695	53.10	521.9	731.1	0.7702
+ A & B & C & D	0.036669	0.8831	0.6729	33.410	63.348	81.48	520.2	729.3	0.7681

Table 8. Ablation study of ROS-FT on the mixed dataset (open, closed, and hybrid surfaces). *Dec.* stands for decoder. *+ A/B/C* indicates fine-tuning the corresponding module with its original loss. *+ D* denotes the addition of the DE-Adapter, which is exclusively trained with the FDG-D representation in Stage 3.

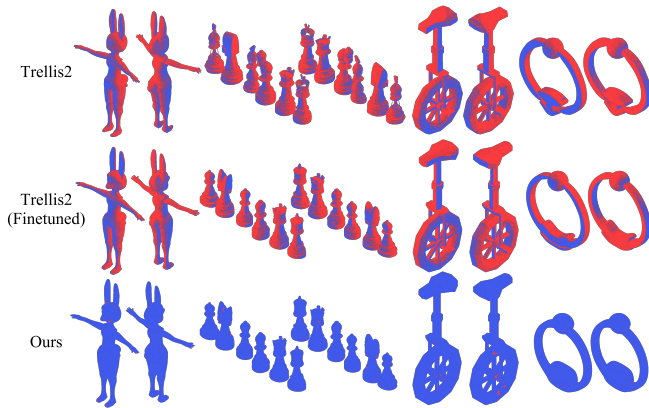


Fig. 10. Qualitative comparison on pure closed surface generation task.

Component	#Params	Share (%)
Sparse structure DiT	1292.18M	41.25
Sparse structure Decoder	73.67M	2.35
Shape DiT	1292.25M	41.25
Shape Decoder	474.23M	15.14
Total	3132.34M	100.00
<b>DE-Adapter (ours)</b>	<b>36.38M</b>	<b>1.16</b>

Table 9. Parameter count breakdown of the 512 *shape-only* inference pipeline (sparse structure DiT/Decoder + shape DiT/Decoder) and the relative size of the our proposed DE-Adapter.

Labs 2026] and ChatGPT Images 2.0 [OpenAI 2026]. As demonstrated in Fig. 14, this synergy allows our method to effortlessly and reliably generate open-surface garments (e.g., pants) alongside their matching closed-surface accessories (e.g., shoes) within one complex outfit. More results are available in our demo video.

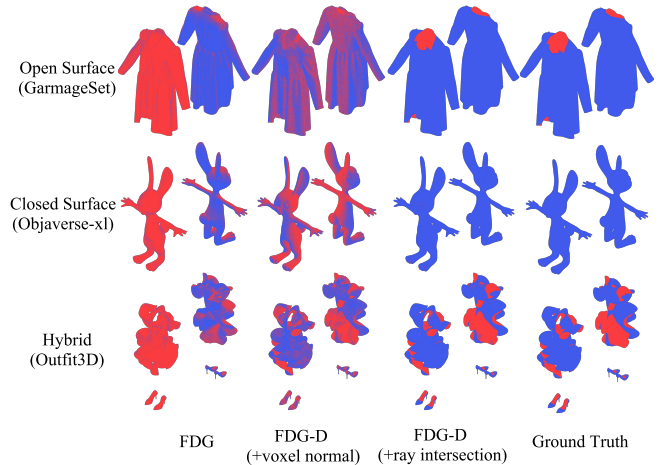


Fig. 11. Ablation study of FDG-D on 3D representation reconstruction task. FDG-D with face normal guidance can significantly improve the normal quality to the ground truth level even in very challenging case (the last row) and ignoring if open surface data or closed surface data.

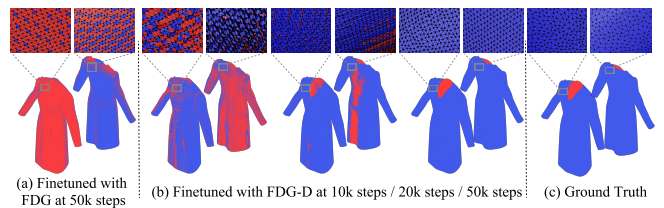


Fig. 12. Ablation study of FDG-D on shape VAE reconstruction task. Shape decoder finetuned with FDG-D can gradually improve the normal quality compared to the baseline FDG still limit in normal quality.

### 6.3 Parameter Efficiency

To demonstrate the lightweight nature of our approach, we provide a parameter count breakdown for the 512-resolution *shape-only* inference pipeline (comprising the sparse structure flow/decoder,

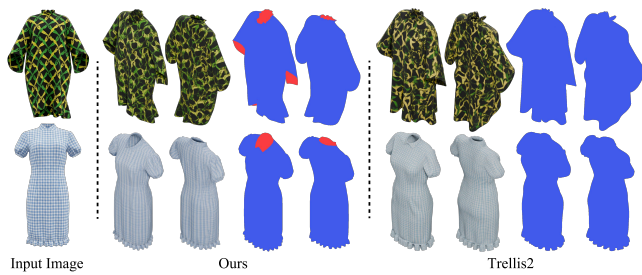


Fig. 13. Our method is compatible with texturing pipeline of Trellis2.

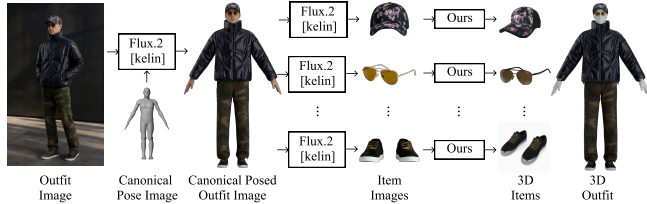


Fig. 14. Multi-item 3D generation with our pipeline can generate open surfaces (pants) and closed surfaces (shoes) for a complex outfit.

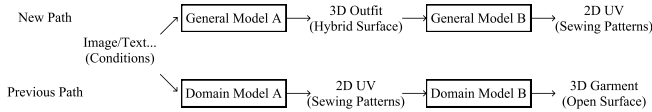


Fig. 15. A new unified pathway for 3D fashion assets generation.

shape flow, and shape decoder). As shown in Tab. 9, our introduced ROS adapter adds only a marginal parameter overhead relative to the frozen base model, ensuring efficient fine-tuning without compromising the generative capabilities of the pre-trained backbone.

#### 6.4 Further Improvements

While our proposed method achieves significant improvements, its performance could be further elevated through two primary scaling directions. First, *Data Scaling*: we finetuned the base model on approximately 10K assets, accounting for only  $\sim 1\%$  of the 970K+ pre-training data used by the base model. Scaling up the high-quality fine-tuning dataset to match the pre-training scale would undoubtedly enhance generalization across more diverse topologies. Second, *Architecture Scaling*: our current DE-Adapter introduces merely  $\sim 1\%$  additional parameters relative to base model. Expanding the parameter size could capture more complex geometric contexts. Ultimately, the most optimal solution might involve designing a similar orientation-aware module natively within the base SC-VAE and incorporating face orientation learning directly into the large-scale pre-training phase, rather than relying solely on post-training.

#### 6.5 Future Directions

Our work establishes a new pathway for 3D fashion modeling by transitioning from domain-specific pattern-stitching to a universal 3D topological generation paradigm. As illustrated in Fig. 15, this new pathway overcomes the fundamental limitations of the

traditional 2D pattern-stitching approach by directly generating open, closed, and hybrid topologies in a unified 3D space. While our proposed method serves as a crucial first step by addressing the normal limitations of general 3D generators (General Model A in Fig. 15), achieving fully controllable, production-ready 3D fashion assets generation remains an open challenge. At the next step, combining our robust 3D outfits with the UV and seam generation techniques—such as PartUV [Wang et al. 2025] and MeshTailor [Ma et al. 2026] (General Model B in Fig. 15)—will pave the way toward a fully automated and universal 3D fashion assets generation pipeline.

## 7 Conclusion

In this work, we present AnySurf, a unified 3D generation pipeline capable of producing open, hybrid, and closed surfaces with accurate face orientations. To overcome the inherent limitations of original FDG representation, we introduce FDG-D (Flexible Dual Grid with Directed Edge), a minimal yet effective 3D representation that preserves critical normal information across diverse topologies. Furthermore, we propose ROS-FT, an efficient post-training strategy utilizing a lightweight DE-Adapter (adding only 1.16% parameters) to significantly enhance normal quality without compromising the base model’s original generative capabilities. To validate our approach and facilitate future research, we construct Outfit3D, an industry-level hybrid dataset featuring high-precision garments and accessories with rich textures and UV information. Extensive experiments demonstrate that AnySurf significantly outperforms existing baselines across diverse surface topologies, evolving 3D fashion generation from an isolated *domain-specific* task into an integral component of the *general* 3D generative landscape.

## References

- Panos Achlioptas, Olga Diamanti, Ioannis Mitliagkas, and Leonidas Guibas. 2018. Learning representations and generative models for 3d point clouds. In *ICML*.
- Siyuan Bian, Chenghao Xu, Yuliang Xiu, Artur Grigorev, Zhen Liu, Cewu Lu, Michael J Black, and Yao Feng. 2025. Chatgarment: Garment estimation, generation and editing via large language models. In *Proceedings of the IEEE/CVF Conference on Computer Vision and Pattern Recognition*. 2924–2934.
- Black Forest Labs. 2026. FLUX.2 [klein] - Fast, Efficient Image Generation. <https://bf.lai/models/flux-2-klein>. 2026-01-21.
- Eric R Chan, Marco Monteiro, Petr Kellnhofer, Jiajun Wu, and Gordon Wetzstein. 2021. pi-gan: Periodic implicit generative adversarial networks for 3d-aware image synthesis.
- Chao Chen, Yu-Shen Liu, and Zhizhong Han. 2024a. Inferring Neural Signed Distance Functions by Overfitting on Single Noisy Point Clouds through Finetuning Data-Driven based Priors. In *Advances in Neural Information Processing Systems*.
- Honghu Chen, Yuxin Yao, and Juyong Zhang. 2024c. Neural-ABC: neural parametric models for articulated body with clothes. *IEEE Transactions on Visualization and Computer Graphics* 31, 2 (2024), 1478–1495.
- Weikai Chen, Cheng Lin, Weiyang Li, and Bo Yang. 2022a. 3psdf: Three-pole signed distance function for learning surfaces with arbitrary topologies. In *Proceedings of the IEEE/CVF Conference on Computer Vision and Pattern Recognition*. 18522–18531.
- Xipeng Chen, Guangrun Wang, Dizhong Zhu, Xiaodan Liang, Philip Torr, and Liang Lin. 2022c. Structure-preserving 3d garment modeling with neural sewing machines. *Advances in Neural Information Processing Systems* 35 (2022), 15147–15159.
- Zhiqin Chen, Andrea Tagliasacchi, Thomas Funkhouser, and Hao Zhang. 2022b. Neural dual contouring. *ACM Transactions on Graphics (TOG)* 41, 4 (2022), 1–13.
- Zhaoxi Chen, Jiaxiang Tang, Yuhao Dong, Ziang Cao, Fangzhou Hong, Yushi Lan, Tengfei Wang, Haozhe Xie, Tong Wu, Shunsuke Saito, et al. 2024b. 3DTopia-XL: Scaling High-quality 3D Asset Generation via Primitive Diffusion. *arXiv preprint arXiv:2409.12957* (2024).
- Zhiqin Chen and Hao Zhang. 2019. Learning implicit fields for generative shape modeling.
- Julian Chibane, Gerard Pons-Moll, et al. 2020. Neural unsigned distance fields for implicit function learning. *Advances in Neural Information Processing Systems* 33 (2020), 21638–21652.

- Matt Deitke, Ruoshi Liu, Matthew Wallingford, Huong Ngo, Oscar Michel, Aditya Kusupati, Alan Fan, Christian Laforte, Vikram Voleti, Samir Yitzhak Gadre, et al. 2024. Objaverse-xl: A universe of 10m+ 3d objects. *Advances in Neural Information Processing Systems* 36 (2024).
- Matt Deitke, Ruoshi Liu, Matthew Wallingford, Huong Ngo, Oscar Michel, Aditya Kusupati, Alan Fan, Christian Laforte, Vikram Voleti, Samir Yitzhak Gadre, Eli VanderBilt, Aniruddha Kembhavi, Carl Vondrick, Georgia Gkioxari, Kiana Ehsani, Ludwig Schmidt, and Ali Farhadi. 2023a. Objaverse-XL: A Universe of 10M+ 3D Objects. In *Thirty-seventh Conference on Neural Information Processing Systems Datasets and Benchmarks Track*. <https://openreview.net/forum?id=Sq3CLKJjeiz>
- Matt Deitke, Dustin Schwenk, Jordi Salvador, Luca Weihs, Oscar Michel, Eli VanderBilt, Ludwig Schmidt, Kiana Ehsani, Aniruddha Kembhavi, and Ali Farhadi. 2023b. Objaverse: A universe of annotated 3d objects. In *Proceedings of the IEEE/CVF Conference on Computer Vision and Pattern Recognition*. 13142–13153.
- Patrick Esser, Sumith Kulal, Andreas Blattmann, Rahim Entezari, Jonas Müller, Harry Saini, Yam Levi, Dominik Lorenz, Axel Sauer, Frederic Boesel, et al. 2024. Scaling rectified flow transformers for high-resolution image synthesis. In *Forty-first international conference on machine learning*.
- Jiatao Gu, Lingjie Liu, Peng Wang, and Christian Theobalt. 2022. Stylenerf: A style-based 3d-aware generator for high-resolution image synthesis.
- Xianfeng Gu, Steven J Gortler, and Hugues Hoppe. 2002. Geometry images. In *Proceedings of the 29th annual conference on Computer graphics and interactive techniques*. 355–361.
- Benoit Guillard, Federico Stella, and Pascal Fua. 2022. MeshUDF: Fast and differentiable meshing of unsigned distance field networks. In *Proceedings of the European Conference on Computer Vision*. Springer, 576–592.
- Jingfeng Guo, Jinnan Chen, Weikai Chen, Zhenyu Sun, Lanjiang Li, Baozhu Zhao, Lingting Zhu, Xin Wang, and Qi Liu. 2025. GarmentX: Autoregressive Parametric Representations for High-Fidelity 3D Garment Generation. *arXiv preprint arXiv:2504.20409* (2025).
- Kai He, Kaixin Yao, Qixuan Zhang, Jingyi Yu, Lingjie Liu, and Lan Xu. 2024. DressCode: Autoregressively Sewing and Generating Garments from Text Guidance. *ACM Transactions on Graphics (TOG)* 43, 4 (2024), 1–13.
- Fei Hou, Xuhui Chen, Wencheng Wang, Hong Qin, and Ying He. 2023. Robust zero level-set extraction from unsigned distance fields based on double covering. *ACM Transactions on Graphics (TOG)* 42, 6 (2023), 1–15.
- Team Hunyuan3D, Shuhui Yang, Mingxin Yang, Yifei Feng, Xin Huang, Sheng Zhang, Zebin He, Di Luo, Haolin Liu, Yunfei Zhao, et al. 2025. Hunyuan3D 2.1: From Images to High-Fidelity 3D Assets with Production-Ready PBR Material. *arXiv preprint arXiv:2506.15442* (2025).
- Tanghai Jia, Dongyu Yan, Dehao Hao, Yang Li, Kaiyi Zhang, Xianyi He, Lanjiang Li, Yuhan Wang, Jinnan Chen, Lutao Jiang, et al. 2025. UltraShape 1.0: High-Fidelity 3D Shape Generation via Scalable Geometric Refinement. *arXiv preprint arXiv:2512.21185* (2025).
- Tao Ju, Frank Losasso, Scott Schaefer, and Joe Warren. 2002. Dual contouring of hermite data. In *Proceedings of the 29th annual conference on Computer graphics and interactive techniques*. 339–346.
- Leif P Kobbelt, Mario Botsch, Ulrich Schwanecke, and Hans-Peter Seidel. 2001. Feature sensitive surface extraction from volume data. In *Proceedings of the 28th annual conference on Computer graphics and interactive techniques*. 57–66.
- Maria Korosteleva, Timur Levent Kesdogan, Fabian Kemper, Stephan Wenninger, Jasmin Koller, Yuhan Zhang, Mario Botsch, and Olga Sorkine-Hornung. 2024. Garment-CodeData: A Dataset of 3D Made-to-Measure Garments With Sewing Patterns. In *Computer Vision – ECCV 2024*.
- Maria Korosteleva and Sung-Hee Lee. 2022. NeuralTailor: Reconstructing Sewing Pattern Structures from 3D Point Clouds of Garments. *ACM Trans. Graph.* 41, 4 (2022), 16 pages. doi:10.1145/3528223.3530179
- Maria Korosteleva and Olga Sorkine-Hornung. 2023. GarmentCode: Programming Parametric Sewing Patterns. *ACM Transaction on Graphics* 42, 6 (2023), 16 pages. doi:10.1145/3618351 SIGGRAPH ASIA 2023 issue.
- Qing Li, Hui Fang Feng, Kanle Shi, Yue Gao, Yi Fang, Yu-Shen Liu, and Zhizhong Han. 2023a. NeuralGF: Unsupervised point normal estimation by learning neural gradient function. *Advances in Neural Information Processing Systems* 36 (2023), 66006–66019.
- Ren Li, Cong Cao, Corentin Dumery, Yingxuan You, Hao Li, and Pascal Fua. 2025a. Single View Garment Reconstruction Using Diffusion Mapping Via Pattern Coordinates. In *Proceedings of the Special Interest Group on Computer Graphics and Interactive Techniques Conference Papers*. 1–11.
- Ren Li, Corentin Dumery, Zhantao Deng, and Pascal Fua. 2024b. Reconstruction of manipulated garment with guided deformation prior. *Advances in Neural Information Processing Systems* 37 (2024), 58637–58662.
- Ren Li, Corentin Dumery, Benoît Guillard, and Pascal Fua. 2024c. Garment Recovery with Shape and Deformation Priors. In *Proceedings of the IEEE/CVF Conference on Computer Vision and Pattern Recognition*. 1586–1595.
- Ren Li, Benoît Guillard, and Pascal Fua. 2024d. Isp: Multi-layered garment draping with implicit sewing patterns. *Advances in Neural Information Processing Systems* 36 (2024).
- Siran Li, Ruiyang Liu, Chen Liu, Zhendong Wang, Gaofeng He, Yong-Lu Li, Xiaogang Jin, and Huamin Wang. 2025c. Garmagenet: A multimodal generative framework for sewing pattern design and generic garment modeling. *ACM Transactions on Graphics (TOG)* 44, 6 (2025), 1–23.
- Shujuan Li, Yu-Shen Liu, and Zhizhong Han. 2025b. Gaussianudf: Inferring unsigned distance functions through 3d gaussian splatting. In *Proceedings of the Computer Vision and Pattern Recognition Conference*. 27113–27123.
- Tianyang Li, Xin Wen, Yu-Shen Liu, Hua Su, and Zhizhong Han. 2022. Learning deep implicit functions for 3D shapes with dynamic code clouds. In *Proceedings of the IEEE/CVF Conference on Computer Vision and Pattern Recognition*. 12840–12850.
- Weiyu Li, Xuanyang Zhang, Zheng Sun, Di Qi, Hao Li, Wei Cheng, Weiwei Cai, Shihao Wu, Jiarui Liu, Zihao Wang, et al. 2025f. Step1x-3d: Towards high-fidelity and controllable generation of textured 3d assets. *arXiv preprint arXiv:2505.07747* (2025).
- Xinyu Li, Qi Yao, and Yuanda Wang. 2025d. GarmentDiffusion: 3D Garment Sewing Pattern Generation with Multimodal Diffusion Transformers. arXiv:2504.21476 [cs.CV] <https://arxiv.org/abs/2504.21476>
- Xuan Li, Chang Yu, Wenxin Du, Ying Jiang, Tianyi Xie, Yunuo Chen, Yin Yang, and Chenfanfu Jiang. 2025e. Dress-1-to-3: Single image to simulation-ready 3d outfit with diffusion prior and differentiable physics. *ACM Transactions on Graphics (TOG)* 44, 4 (2025), 1–16.
- Yifei Li, Hsiao-yu Chen, Egor Larionov, Nikolaos Sarafianos, Wojciech Matusik, and Tuur Stuyck. 2024a. Diffavator: Simulation-ready garment optimization with differentiable simulation. In *Proceedings of the IEEE/CVF Conference on Computer Vision and Pattern Recognition*. 4368–4378.
- Yangguang Li, Zi-Xin Zou, Zexiang Liu, Dehu Wang, Yuan Liang, Zhipeng Yu, Xingchao Liu, Yuan-Chen Guo, Ding Liang, Wanli Ouyang, et al. 2025g. Tripog: High-fidelity 3d shape synthesis using large-scale rectified flow models. *IEEE Transactions on Pattern Analysis and Machine Intelligence* (2025).
- Zhaoshuo Li, Thomas Müller, Alex Evans, Russell H Taylor, Mathias Unberath, Ming-Yu Liu, and Chen-Hsuan Lin. 2023b. Neuralangelo: High-Fidelity Neural Surface Reconstruction. In *Proceedings of the IEEE/CVF Conference on Computer Vision and Pattern Recognition*. 8456–8465.
- Yuchen Lin, Chenguo Lin, Panwang Pan, Honglei Yan, Feng Yiqiang, Yadong MU, and Katerina Fragkiadaki. [n. d.]. PartCrafter: Structured 3D Mesh Generation via Compositional Latent Diffusion Transformers. In *The Thirty-ninth Annual Conference on Neural Information Processing Systems*.
- Yaron Lipman, Ricky TQ Chen, Heli Ben-Hamu, Maximilian Nickel, and Matthew Le. 2023. Flow Matching for Generative Modeling. In *ICLR*.
- Anran Liu, Cheng Lin, Yuan Liu, Xiaoxiao Long, Zhiyang Dou, Hao-Xiang Guo, Ping Luo, and Wenping Wang. 2024b. Part123: Part-aware 3D Reconstruction from a Single-view Image. *arXiv preprint arXiv:2405.16888* (2024).
- Lijuan Liu, Xiangyu Xu, Zhijie Lin, Jiabin Liang, and Shuicheng Yan. 2023b. Towards Garment Sewing Pattern Reconstruction from a Single Image. *ACM Transactions on Graphics (SIGGRAPH Asia)* (2023).
- Shengqi Liu, Yuhao Cheng, Zhuo Chen, Xingyu Ren, Wenhan Zhu, Lincheng Li, Mengxiao Bi, Xiaokang Yang, and Yichao Yan. 2025. Multimodal latent diffusion model for complex sewing pattern generation. In *Proceedings of the IEEE/CVF International Conference on Computer Vision*. 17640–17650.
- Yuan Liu, Cheng Lin, Zijiao Zeng, Xiaoxiao Long, Lingjie Liu, Taku Komura, and Wenping Wang. 2023a. SyncDreamer: Generating Multiview-consistent Images from a Single-view Image. *arXiv preprint arXiv:2309.03453* (2023).
- Yufei Liu, Junshu Tang, Chu Zheng, Shijie Zhang, Jinkun Hao, Junwei Zhu, and Dongjin Huang. 2024c. ClotheDreamer: Text-Guided Garment Generation with 3D Gaussians. arXiv:2406.16815 [cs.CV]
- Zhen Liu, Yao Feng, Yuliang Xiu, Weiyang Liu, Liam Paull, Michael J Black, and Bernhard Schölkopf. 2024a. Ghost on the Shell: An Expressive Representation of General 3D Shapes. In *ICLR*.
- Xiaoxiao Long, Yuan-Chen Guo, Cheng Lin, Yuan Liu, Zhiyang Dou, Lingjie Liu, Yuexin Ma, Song-Hai Zhang, Marc Habermann, Christian Theobalt, et al. 2023a. Wonder3D: Single Image to 3D using Cross-Domain Diffusion. *arXiv preprint arXiv:2310.15008* (2023).
- Xiaoxiao Long, Cheng Lin, Lingjie Liu, Yuan Liu, Peng Wang, Christian Theobalt, Taku Komura, and Wenping Wang. 2023b. NeuralUDF: Learning unsigned distance fields for multi-view reconstruction of surfaces with arbitrary topologies. In *Proceedings of the IEEE/CVF Conference on Computer Vision and Pattern Recognition*. 20834–20843.
- William E Lorensen and Harvey E Cline. 1998. Marching cubes: A high resolution 3D surface construction algorithm. In *Seminal graphics: pioneering efforts that shaped the field*. 347–353.
- Shitong Luo and Wei Hu. 2021. Diffusion probabilistic models for 3d point cloud generation. In *Proceedings of the IEEE/CVF Conference on Computer Vision and Pattern Recognition*. 2837–2845.
- Zhongjin Luo, Haolin Liu, Chenghong Li, Wanghao Du, Zirong Jin, Wanhu Sun, Yinyu Nie, Weikai Chen, and Xiaoguang Han. 2024. GarVerseLOD: High-Fidelity 3D Garment Reconstruction from a Single In-the-Wild Image using a Dataset with Levels of Details. *ACM Transactions on Graphics (TOG)* (2024).

- Baorui Ma, Zhizhong Han, Yu-Shen Liu, and Matthias Zwicker. 2021. Neural-Pull: Learning Signed Distance Function from Point clouds by Learning to Pull Space onto Surface. In *International Conference on Machine Learning*. PMLR, 7246–7257.
- Xueqi Ma, Xingguang Yan, Congyue Zhang, and Hui Huang. 2026. MeshTailor: Cutting Seams via Generative Mesh Traversal. arXiv:2603.27309 [cs.GR] <https://arxiv.org/abs/2603.27309>
- Lars Mescheder, Michael Oechsle, Michael Niemeyer, Sebastian Nowozin, and Andreas Geiger. 2019. Occupancy networks: Learning 3D reconstruction in function space. In *Proceedings of the IEEE/CVF Conference on Computer Vision and Pattern Recognition*. 4460–4470.
- Paritosh Mittal, Yen-Chi Cheng, Maneesh Singh, and Shubham Tulsiani. 2022. AutoSDF: Shape Priors for 3D Completion, Reconstruction and Generation. In *CVPR*.
- Kiyohiro Nakayama, Jan Ackermann, Timur Levent Kesdogan, Yang Zheng, Maria Korosteleva, Olga Sorkine-Hornung, Leonidas Guibas, Guandao Yang, and Gordon Wetzstein. 2024. AIpparel: A Large Multimodal Generative Model for Digital Garments. *arXiv preprint arXiv:2412.03937* (2024).
- Takeshi Noda, Chao Chen, Xinhai Liu, Weiqi Zhang and, Yu-Shen Liu, and Zhizhong Han. 2024. MultiPull: Detailing Signed Distance Functions by Pulling Multi-Level Queries at Multi-Step. In *Advances in Neural Information Processing Systems*.
- OpenAI. 2026. ChatGPT Images 2.0. <https://openai.com/zh-Hans-CN/index/introducing-chatgpt-images-2-0/>. 2026-04-21.
- Jeong Joon Park, Peter Florence, Julian Straub, Richard Newcombe, and Steven Lovegrove. 2019. DeepSDF: Learning continuous signed distance functions for shape representation. In *Proceedings of the IEEE/CVF Conference on Computer Vision and Pattern Recognition*. 165–174.
- Lingteng Qiu, Guanying Chen, Jiapeng Zhou, Mutian Xu, Junle Wang, and Xiaoguang Han. 2023. Rec-mv: Reconstructing 3d dynamic cloth from monocular videos. In *Proceedings of the IEEE/CVF Conference on Computer Vision and Pattern Recognition*. 4637–4646.
- Boxiang Rong, Artur Grigorev, Wenbo Wang, Michael J Black, Bernhard Thomaszewski, Christina Tsalicoglou, and Otmar Hilliges. 2025. Gaussian garments: Reconstructing simulation-ready clothing with photorealistic appearance from multi-view video. In *2025 International Conference on 3D Vision (3DV)*. IEEE, 1054–1063.
- Nikolaos Sarafianos, Tuur Stuyck, Xiaoyu Xiang, Yilei Li, Jovan Popovic, and Rakesh Ranjan. 2024. Garment3dgen: 3d garment stylization and texture generation. *arXiv preprint arXiv:2403.18816* (2024).
- Tianchang Shen, Jacob Munkberg, Jon Hasselgren, Kangxue Yin, Zian Wang, Wenzheng Chen, Zan Gojcic, Sanja Fidler, Nicholas Sharp, and Jun Gao. 2023. Flexible isosurface extraction for gradient-based mesh optimization. *ACM Transactions on Graphics (TOG)* 42, 4 (2023), 1–16.
- Wenda Shi, Yiren Song, Zihan Rao, Dengming Zhang, Jiaming Liu, and Xingxing Zou. 2026. WordCon: Word-level Typography Control in Visual Text Rendering. *IEEE Transactions on Circuits and Systems for Video Technology* (2026), 1–1. doi:10.1109/TCSVT.2026.3686871
- Wenda Shi, Yiren Song, Dengming Zhang, Jiaming Liu, and Xingxing Zou. 2025. FonTS: Text Rendering With Typography and Style Controls. In *Proceedings of the IEEE/CVF International Conference on Computer Vision (ICCV)*. 18463–18474.
- Edward J Smith and David Meger. 2017. Improved adversarial systems for 3d object generation and reconstruction.
- Jiaming Sun, Yiming Xie, Linghao Chen, Xiaowei Zhou, and Hujun Bao. 2021. NeuralRecon: Real-time coherent 3D reconstruction from monocular video. In *Proceedings of the IEEE/CVF Conference on Computer Vision and Pattern Recognition*. 15598–15607.
- Yuki Tatsukawa, Anran Qi, I-Chao Shen, and Takeo Igarashi. 2025. GarmentImage: Raster Encoding of Garment Sewing Patterns with Diverse Topologies. In *Proceedings of the Special Interest Group on Computer Graphics and Interactive Techniques Conference Papers*. 1–11.
- Dmitry Tochilkin, David Pankratz, Zexiang Liu, Zixuan Huang, Adam Letts, Yangguang Li, Ding Liang, Christian Laforte, Varun Jampani, and Yan-Pei Cao. 2024. Triposr: Fast 3d object reconstruction from a single image. *arXiv preprint arXiv:2403.02151* (2024).
- Peng Wang, Lingjie Liu, Yuan Liu, Christian Theobalt, Taku Komura, and Wenping Wang. 2021. NeuS: Learning neural implicit surfaces by volume rendering for multi-view reconstruction. In *Advances in Neural Information Processing Systems*. 27171–27183.
- Zhaoning Wang, Xinyue Wei, Ruoxi Shi, Xiaoshuai Zhang, Hao Su, and Minghua Liu. 2025. PartUV: Part-Based UV Unwrapping of 3D Meshes. In *Proceedings of the SIGGRAPH Asia 2025 Conference Papers (SA Conference Papers '25)*. Association for Computing Machinery, New York, NY, USA, Article 15, 12 pages. doi:10.1145/3757377.3763843
- Jianfeng Xiang, Xiaoxue Chen, Sicheng Xu, Ruicheng Wang, Zelong Lv, Yu Deng, Hongyuan Zhu, Yue Dong, Hao Zhao, Nicholas Jing Yuan, et al. 2025a. Native and compact structured latents for 3d generation. *arXiv preprint arXiv:2512.14692* (2025).
- Jianfeng Xiang, Zelong Lv, Sicheng Xu, Yu Deng, Ruicheng Wang, Bowen Zhang, Dong Chen, Xin Tong, and Jiaolong Yang. 2025b. Structured 3d latents for scalable and versatile 3d generation. In *Proceedings of the IEEE/CVF conference on computer vision and pattern recognition*. 21469–21480.
- Jianwen Xie, Zilong Zheng, Ruiqi Gao, Wenguan Wang, Song-Chun Zhu, and Ying Nian Wu. 2018. Learning descriptor networks for 3d shape synthesis and analysis.
- Tianyi Xie, Zeshun Zong, Yuxing Qiu, Xuan Li, Yutao Feng, Yin Yang, and Chenfanfu Jiang. 2024. Physgaussian: Physics-integrated 3d gaussians for generative dynamics. In *Proceedings of the IEEE/CVF Conference on Computer Vision and Pattern Recognition*. 4389–4398.
- Xingguang Yan, Han-Hung Lee, Ziyu Wan, and Angel X Chang. 2024. An object is worth 64x64 pixels: Generating 3d object via image diffusion. *arXiv preprint arXiv:2408.03178* (2024).
- Xingguang Yan, Han-Hung Lee, Ziyu Wan, and Angel X Chang. 2025. An object is worth 64x 64 pixels: Generating 3d object via image diffusion. In *2025 International Conference on 3D Vision (3DV)*. IEEE, 123–133.
- Jiayu Yang, Taizhang Shang, Weixuan Sun, Xibin Song, Ziang Cheng, Senbo Wang, Shenzhou Chen, Weizhe Liu, Hongdong Li, and Pan Ji. 2025a. Pandora3d: A comprehensive framework for high-quality 3d shape and texture generation. *arXiv preprint arXiv:2502.14247* (2025).
- Xianghui Yang, Huiwen Shi, Bowen Zhang, Fan Yang, Jiacheng Wang, Hongxu Zhao, Xinhai Liu, Xinzhou Wang, Qingxiang Lin, Jiaao Yu, et al. 2024. Hunyuan3d 1.0: A unified framework for text-to-3d and image-to-3d generation. *arXiv preprint arXiv:2411.02293* (2024).
- Yunhan Yang, Yufan Zhou, Yuan-Chen Guo, Zi-Xin Zou, Yukun Huang, Ying-Tian Liu, Hao Xu, Ding Liang, Yan-Pei Cao, and Xihui Liu. 2025b. Omnipart: Part-aware 3d generation with semantic decoupling and structural cohesion. In *Proceedings of the SIGGRAPH Asia 2025 Conference Papers*. 1–12.
- Jingfeng Yao, Bin Yang, and Xingguang Wang. 2025. Reconstruction vs. generation: Taming optimization dilemma in latent diffusion models. In *Proceedings of the Computer Vision and Pattern Recognition Conference*. 15703–15712.
- Hu Ye, Jun Zhang, Sibo Liu, Xiao Han, and Wei Yang. 2023. IP-Adapter: Text Compatible Image Prompt Adapter for Text-to-Image Diffusion Models. arXiv:2308.06721 [cs.CV] <https://arxiv.org/abs/2308.06721>
- Jiawang Yu and Zhenqiang Wang. 2024. Super-Resolution Cloth Animation with Spatial and Temporal Coherence. *ACM Transactions on Graphics (TOG)* 43, 4 (2024), 1–14.
- Zhengming Yu, Zhiyang Dou, Xiaoxiao Long, Cheng Lin, Zekun Li, Yuan Liu, Norman Müller, Taku Komura, Marc Habermann, Christian Theobalt, et al. 2025. Surf-D: Generating High-Quality Surfaces of Arbitrary Topologies Using Diffusion Models. In *European Conference on Computer Vision*. Springer, 419–438.
- Biao Zhang, Jiapeng Tang, Matthias Niessner, and Peter Wonka. 2023b. 3dshape2vecset: A 3d shape representation for neural fields and generative diffusion models. *ACM Transactions On Graphics (TOG)* 42, 4 (2023), 1–16.
- Lvmin Zhang, Anyi Rao, and Maneesh Agrawala. 2023a. Adding Conditional Control to Text-to-Image Diffusion Models. In *2023 IEEE/CVF International Conference on Computer Vision (ICCV)*. 3813–3824. doi:10.1109/ICCV51070.2023.00355
- Longwen Zhang, Ziyu Wang, Qixuan Zhang, Qiwei Qiu, Anqi Pang, Haoran Jiang, Wei Yang, Lan Xu, and Jingyi Yu. 2024b. CLAY: A Controllable Large-scale Generative Model for Creating High-quality 3D Assets. *ACM Transactions on Graphics (TOG)* 43, 4 (2024), 1–20.
- Wenyuan Zhang, Kanle Shi, Yu-Shen Liu, and Zhizhong Han. 2024a. Learning unsigned distance functions from multi-view images with volume rendering priors. In *Proceedings of the European Conference on Computer Vision*.
- Yibo Zhang, Li Zhang, Rui Ma, and Nan Cao. 2025. TexVerse: A Universe of 3D Objects with High-Resolution Textures. *arXiv preprint arXiv:2508.10868* (2025).
- Zibo Zhao, Zeqiang Lai, Qingxiang Lin, Yunfei Zhao, Haolin Liu, Shuhui Yang, Yifei Feng, Mingxin Yang, Sheng Zhang, Xianghui Yang, et al. 2025. Hunyuan3d 2.0: Scaling diffusion models for high resolution textured 3d assets generation. *arXiv preprint arXiv:2501.12202* (2025).
- Boyang Zheng, Nanye Ma, Shengbang Tong, and Saining Xie. 2025. Diffusion transformers with representation autoencoders. *arXiv preprint arXiv:2510.11690* (2025).
- Feng Zhou, Ruiyang Liu, Chen Liu, Gaofeng He, Yong-Lu Li, Xiaogang Jin, and Huamin Wang. 2025. Design2GarmentCode: Turning design concepts to tangible garments through program synthesis. In *Proceedings of the Computer Vision and Pattern Recognition Conference*. 23712–23722.
- Junsheng Zhou, Baorui Ma, Shujuan Li, Yu-Shen Liu, Yi Fang, and Zhizhong Han. 2024. CAP-UDF: Learning Unsigned Distance Functions Progressively from Raw Point Clouds with Consistency-Aware Field Optimization. *IEEE Transactions on Pattern Analysis and Machine Intelligence* 01 (2024), 1–18.
- Heming Zhu, Lingteng Qiu, Yuda Qiu, and Xiaoguang Han. 2022. Registering explicit to implicit: Towards high-fidelity garment mesh reconstruction from single images. In *Proceedings of the IEEE/CVF Conference on Computer Vision and Pattern Recognition*. 3845–3854.
- Xingxing Zou, Xintong Han, and Waikewong Wong. 2023. Cloth4d: A dataset for clothed human reconstruction. In *Proceedings of the IEEE/CVF Conference on Computer Vision and Pattern Recognition*. 12847–12857.

Received 20 February 2007; revised 12 March 2009; accepted 5 June 2009